Resource

Cell

A Cellular Taxonomy of the Bone Marrow Stroma in Homeostasis and Leukemia

Graphical Abstract

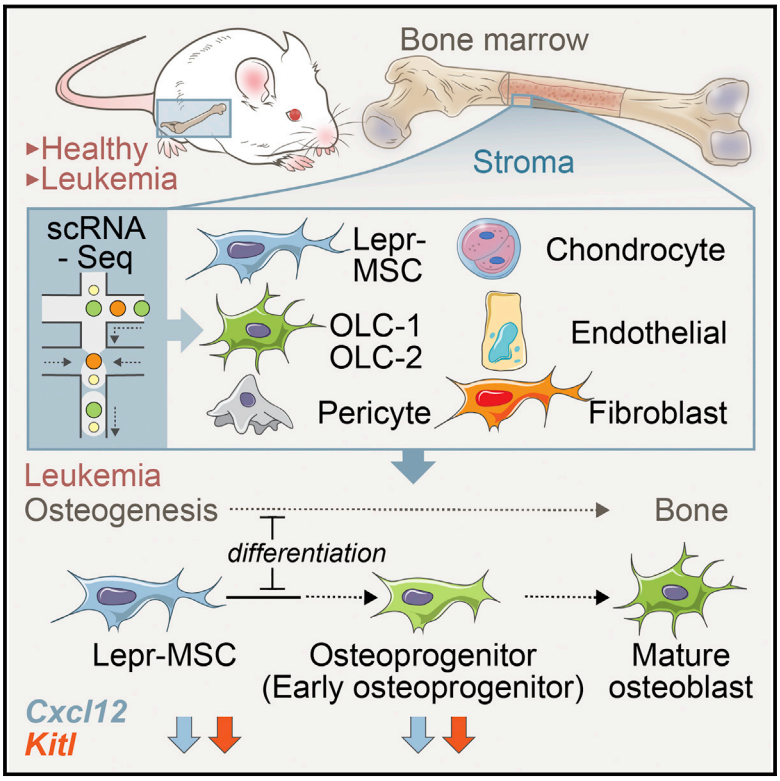

Highlights

- A single-cell bone marrow stromal cell atlas at steady-state and emergent leukemia
- A portal for comparative cell and molecular analyses of bone marrow stromal cells
- Distinction among putative niche cells and types of osteolineage differentiation
- Leukemia remodeling of stroma to the disadvantage of normal hematopoietic cells

Authors

Ninib Baryawno, Dariusz Przybylski, Monika S. Kowalczyk, ..., Orit Rozenblatt-Rosen, Aviv Regev, David T. Scadden

Correspondence

aregev@broadinstitute.org (A.R.), david_scadden@harvard.edu (D.T.S.)

In Brief

Molecular definition of the cell populations comprising bone marrow stroma is provided with single-cell resolution. Seventeen distinct cell subsets with new mesenchymal, pericyte, fibroblast, and endothelial subpopulations, new inferred osteolineage differentiation trajectories, and distinctions among Lepr, Nestin, and NG2-expressing HSC niche populations are defined. The changes imposed by an emergent AML indicate impaired stromal differentiation among mesenchymal cells and decreased expression of hematopoietic regulatory genes consistent with cancer cells indirectly impairing the normal hematopoietic cells with whom they must compete.

Baryawno et al., 2019, Cell *177*, 1915–1932
June 13, 2019
https://doi.org/10.1016/j.cell.2019.04.040

CellPress

Resource

Cell

A Cellular Taxonomy of the Bone Marrow Stroma in Homeostasis and Leukemia

Ninib Baryawno,[1,2,3,4,9] Dariusz Przybylski,[5,9] Monika S. Kowalczyk,[5,9] Youmna Kfoury,[1,2,3] Nicolas Severe,[1,2,3] Karin Gustafsson,[1,2,3] Konstantinos D. Kokkaliaris,[1,2,3] Francois Mercier,[1,2,3] Marcin Tabaka,[5] Matan Hofree,[5] Danielle Dionne,[5] Ani Papazian,[1,2,3] Dongjun Lee,[1,2,3,6] Orr Ashenberg,[5] Ayshwarya Subramanian,[5] Eeshit Dhaval Vaishnav,[5] Orit Rozenblatt-Rosen,[5] Aviv Regev,[5,7,8,*] and David T. Scadden[1,2,3,8,10,*]

[1]Center for Regenerative Medicine, Massachusetts General Hospital, Boston, MA 02114, USA
[2]Harvard Stem Cell Institute, Cambridge, MA 02138, USA
[3]Department of Stem Cell and Regenerative Biology, Harvard University, Cambridge, MA 02138, USA
[4]Childhood Cancer Research Unit, Dep. of Children's and Women's Health, Karolinska Institutet, 171 77 Stockholm, Sweden
[5]Klarman Cell Observatory, Broad Institute of Harvard and MIT, Cambridge, MA 02142, USA
[6]Department of Convergence Medical Science, Pusan National University School of Medicine, Yangsan 50612, Republic of Korea
[7]Howard Hughes Medical Institute, Koch Institute of Integrative Cancer Research, Department of Biology, Massachusetts Institute of Technology, Cambridge, MA 02142, USA
[8]Senior author
[9]These authors contributed equally
[10]Lead Contact
*Correspondence: aregev@broadinstitute.org (A.R.), david_scadden@harvard.edu (D.T.S.)
https://doi.org/10.1016/j.cell.2019.04.040

SUMMARY

Stroma is a poorly defined non-parenchymal component of virtually every organ with key roles in organ development, homeostasis, and repair. Studies of the bone marrow stroma have defined individual populations in the stem cell niche regulating hematopoietic regeneration and capable of initiating leukemia. Here, we use single-cell RNA sequencing (scRNA-seq) to define a cellular taxonomy of the mouse bone marrow stroma and its perturbation by malignancy. We identified seventeen stromal subsets expressing distinct hematopoietic regulatory genes spanning new fibroblastic and osteoblastic subpopulations including distinct osteoblast differentiation trajectories. Emerging acute myeloid leukemia impaired mesenchymal osteogenic differentiation and reduced regulatory molecules necessary for normal hematopoiesis. These data suggest that tissue stroma responds to malignant cells by disadvantaging normal parenchymal cells. Our taxonomy of the stromal compartment provides a comprehensive bone marrow cell census and experimental support for cancer cell crosstalk with specific stromal elements to impair normal tissue function and thereby enable emergent cancer.

INTRODUCTION

Stem cell niches are a tissue microenvironment that maintains and regulates stem cell function through cellular interactions and secreted factors (Schofield, 1978; Scadden, 2014). Hematopoiesis provides a paradigm for understanding mammalian stem cell niches with pivotal knowledge from numerous *in vivo* studies on the critical role of specific non-hematopoietic, stromal cells in regulating hematopoietic stem cell (HSC) function (Calvi et al., 2003; Ding et al., 2012; Kunisaki et al., 2013; Méndez-Ferrer et al., 2010; Zhang et al., 2003).

One major component is multipotent mesenchymal stem/stromal cells (MSCs), non-hematopoietic cells derived from the mesoderm with potential to differentiate into bone, fat, and cartilage *in vitro* (Kfoury and Scadden, 2015). While MSCs are found in most tissues, their diversity and lineage relationships are incompletely understood. For instance, several subtypes of MSCs that regulate HSCs have been described in specialized bone niches. Most of them are located in the perivascular space and are associated with arteriole or sinusoidal blood vessels, and produce key HSC niche factors such as Cxcl12 and stem cell factor (SCF, also named *Kitl*) (Morrison and Scadden, 2014). They are identified by expression of leptin receptor (Lepr) (Ding and Morrison, 2013; Ding et al., 2012), Nestin (*Nes*) (Méndez-Ferrer et al., 2010), or NG2 (*Cspg4*) (Kunisaki et al., 2013) and were mostly studied in Lepr-cre, Nes-GFP, and NG2-CreER reporter lines, respectively. However, the Lepr-cre (Zhou et al., 2014a) and Nes-GFP (Méndez-Ferrer et al., 2010) are non-inducible mouse lines with expression throughout development or with discrepancy between expression of the marker gene and that of the endogenous locus. Therefore, it is unclear if these markers delineate distinct or overlapping cell populations. Other non-hematopoietic cells, including bone marrow-derived endothelial cells (BMECs) and MSC-descendent osteolineage cells (OLCs), also function as niche cells. BMECs produce Cxcl12 and Kitl and are critical regulators of HSC function (Butler et al., 2010; Ding et al., 2012; Doan et al., 2013; Hooper et al., 2009; Itkin et al., 2016; Kobayashi et al., 2010; Kusumbe et al., 2016). OLCs are critical for HSC homing after lethal irradiation and bone marrow transplantation (Lo Celso et al., 2009),

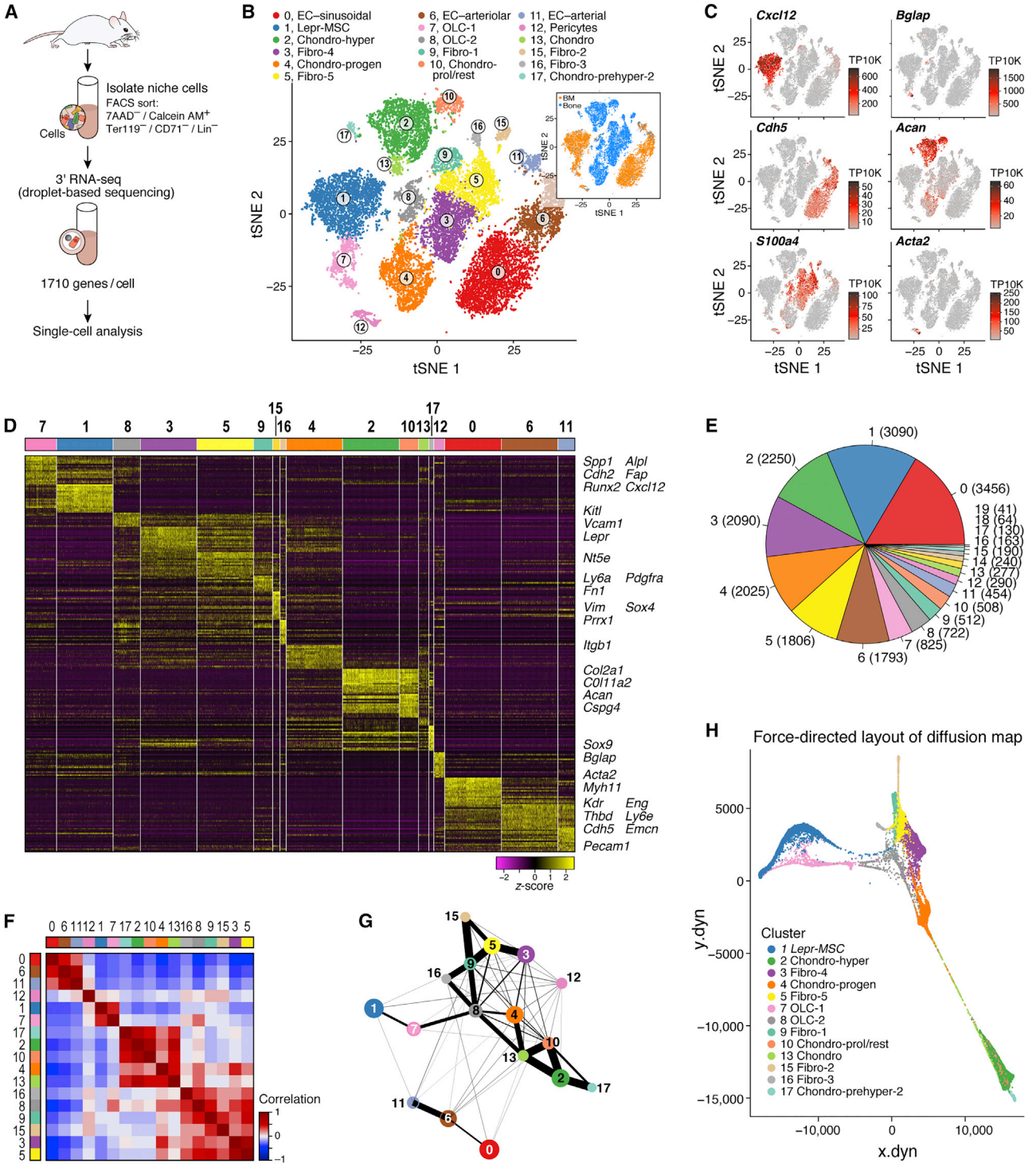

Figure 1. A Single-Cell Atlas of the Mouse Bone Marrow Stroma

(A) Study overview.

(B and C) Seventeen bone marrow stroma cell clusters. t-Distributed stochastic neighbor embedding (t-SNE) of 20,896 non-hematopoietic cells (mixed bone and bone marrow fractions, n = 6 mice), annotated post hoc and colored by clustering, bone or bone marrow location (inset) (B) or by expression (color bar, TP10K) of key cell-type marker genes (C).

(D) Cluster signature genes. Expression (row-wide *Z* score of ln(TP10K+1)) of top differentially expressed genes (rows) across the cells (columns) in each cluster (color bar, top, as in B). The largest clusters were down-sampled. Key genes highlighted on right.

(legend continued on next page)

modulate hematopoietic progenitor function and lineage maturation (Ding and Morrison, 2013; Yu et al., 2016; Yu et al., 2015), and dysfunction in some of them has been implicated in the development of myelodysplasia and leukemia (Dong et al., 2016; Kode et al., 2014; Raaijmakers et al., 2010; Zambetti et al., 2016).

Despite extensive studies, a comprehensive analysis of bone marrow stromal cells is missing, limiting our ability to prospectively isolate and functionally characterize niche cells. Previous profiling studies used reporter genes to purify bulk cell populations (Morrison and Scadden, 2014), which necessarily underestimate cell complexity and restrict analysis in a marker-biased manner.

Here, we use single-cell RNA sequencing (scRNA-seq) to chart a comprehensive census of the bone marrow stroma. We identified 17 distinct cell subsets and their gene signatures, and defined stromal cells expressing key niche factors at steady-state hematopoiesis. We further inferred their differentiation relationships and characterized diversity within specific cell types. Finally, we dissected the global influence of developing acute myeloid leukemia (AML) on the bone marrow microenvironment and described resulting cellular and molecular abnormalities.

RESULTS

A scRNA-Seq Census of Bone Marrow Stroma Identifies Six Distinct Cell Populations and Their Differentiation Relations

To explore the cellular composition of the mouse bone marrow stroma, we profiled non-hematopoietic bone marrow cells from C57BL/6 mice (n = 14) by droplet-based scRNA-seq (Figures 1A, 1B, and S1A–S1E). Unbiased clustering of the stroma resulted in 17 clusters originating from bone or bone marrow (Figure 1B, inset; Table S1), spanning MSCs, OLCs, chondrocytes, fibroblasts, BMECs, and pericytes and possible transitional states (Figures 1B–1H and S1F–S1H). In particular, there were: (1) MSCs (cluster 1, expressing *Lepr*) (Ding and Morrison, 2013) and *Cxcl12* (Greenbaum et al., 2013); (2) two OLC subsets (clusters 7 and 8, expressing osteocalcin [*Bglap*]) (Delmas et al., 1986); (3) four chondrocyte subsets (clusters 2, 10, 13, and 17; expressing the chondrocyte markers, aggrecan [*Acan*]) (Doege et al., 1991) and *Col2a1* (Chan et al., 1995); (4) five fibroblasts subsets (clusters 3, 5, 9, 15, and 16; expressing fibroblast-specific protein-1 [*S100a4*]) (Strutz et al., 1995); (5) three BMEC subsets (clusters 0, 6, and 11; expressing the pan-endothelial marker Ve-cadherin [*Cdh5*]) (Corada et al., 2001); (6) pericytes (cluster 12, expressing alpha smooth muscle actin [*Acta2*]) (Armulik et al., 2011); and (7) clusters 4 and 8, expressing markers of chondrocytes, osteoblasts, and fibroblasts. Fibroblasts, OLCs, and chondrocytes had the lowest proliferation status (Figure S1I).

To help resolve differentiation relations among cells we used correlations of average expression profiles between clusters (Figure 1F), graph abstraction (Wolf et al., 2017) (Figure 1G), and diffusion map analysis (Schiebinger et al., 2017) (Figures 1H and S1F). We discuss these below in the context of each lineage and differentiation path.

We validated two of the most abundant subsets, MSCs and BMECs, by fluorescence-activated cell sorting (FACS), showing that the four clusters can be partitioned prospectively by using antibodies that label BMECs (CD31, Sca-1(*Ly6a*), CD34, Cdh5) or MSCs (CD106) (Figures S1G, S1K, and S1L).

Lepr-MSCs Produce HSC Regulators and Partition into Subsets Spanning a Differentiation Continuum

The prevailing model of MSCs in the bone marrow is that of a multipotent stem cell that can differentiate into bone cells, adipocytes, and chondrocytes (Dominici et al., 2006), but their exact identity remains unclear. While many protein markers have been proposed and deployed in mice (e.g., Cxcl12, Lepr, Nes, NG2) (Ding and Morrison, 2013; Ding et al., 2012; Kunisaki et al., 2013; Méndez-Ferrer et al., 2010; Sugiyama et al., 2006) or humans (CD73 [*Nt5e*], CD106 [*Vcam1*] [Mabuchi et al., 2013], CD105 [*Eng*] [Dominici et al., 2006], or CD90 [*Thy1*] [Pittenger et al., 1999]), there is no single accepted combination and some may also be expressed by pericytes, BMECs, and chondrocytes (Kfoury and Scadden, 2015). We hypothesized that more comprehensive transcriptional profiles will better identify subsets and relate them to legacy markers.

We annotated cluster 1 (Figure 2A) as Lepr^{+} mesenchymal stromal cells (hereafter referred to as Lepr-MSCs) with pre-adipocytic features. First, the cells highly expressed *Lepr*, a perivascular MSC marker (Ding et al., 2012; Morrison and Scadden, 2014), adiponectin (*Adipoq*), a gene highly expressed in preadipocytes (Lara-Castro et al., 2007), and the key HSC niche factors *Cxcl12*, *Kitl*, and angiopoietin-1 (*Angpt1*) (Figures 2B, 2C, and S2C). The cells expressed MSC markers (*Nt5e*, *Vcam1*, and *Eng*) as well as *Grem1*, a marker of mouse skeletal stem cells (Worthley et al., 2015) (Figures S2A and S2C). Other previously proposed MSC markers, such as *Thy1*, *Ly6a*, and the perivascular MSC markers *Nes* and *NG2* (*Cspg4*), were not expressed in cluster 1, but were expressed in other clusters. This indicated the potential for MSC activity in other clusters (Figures S2A–S2C). Our designation of mesenchymal *stromal* cells does not preclude the functional attributes of mesenchymal *stem* cells in other stromal populations. Our taxonomy was based on gene expression with annotations of putative functions; current methods do not allow *in vivo* functional assessment of each cell cluster.

(E) Number of cells in each subset. Color bar as in (B).
(F and G) Differentiation relations between cells or clusters.
(F) Pearson's correlation (color bar) between the average gene expression profiles of clusters (rows, columns, color code as in B).
(G) Relatedness (edges, width indicates strength) between clusters (nodes, colored as in B) based on cluster graph abstraction.
(H) A force directed layout embedding (FLE) of the cells (dots) from a diffusion map (50 components) computed with the cells from strongly connected clusters (as indicated in G and F, without clusters 1, 6, 11, and 12).
See also Figure S1 and Table S1.

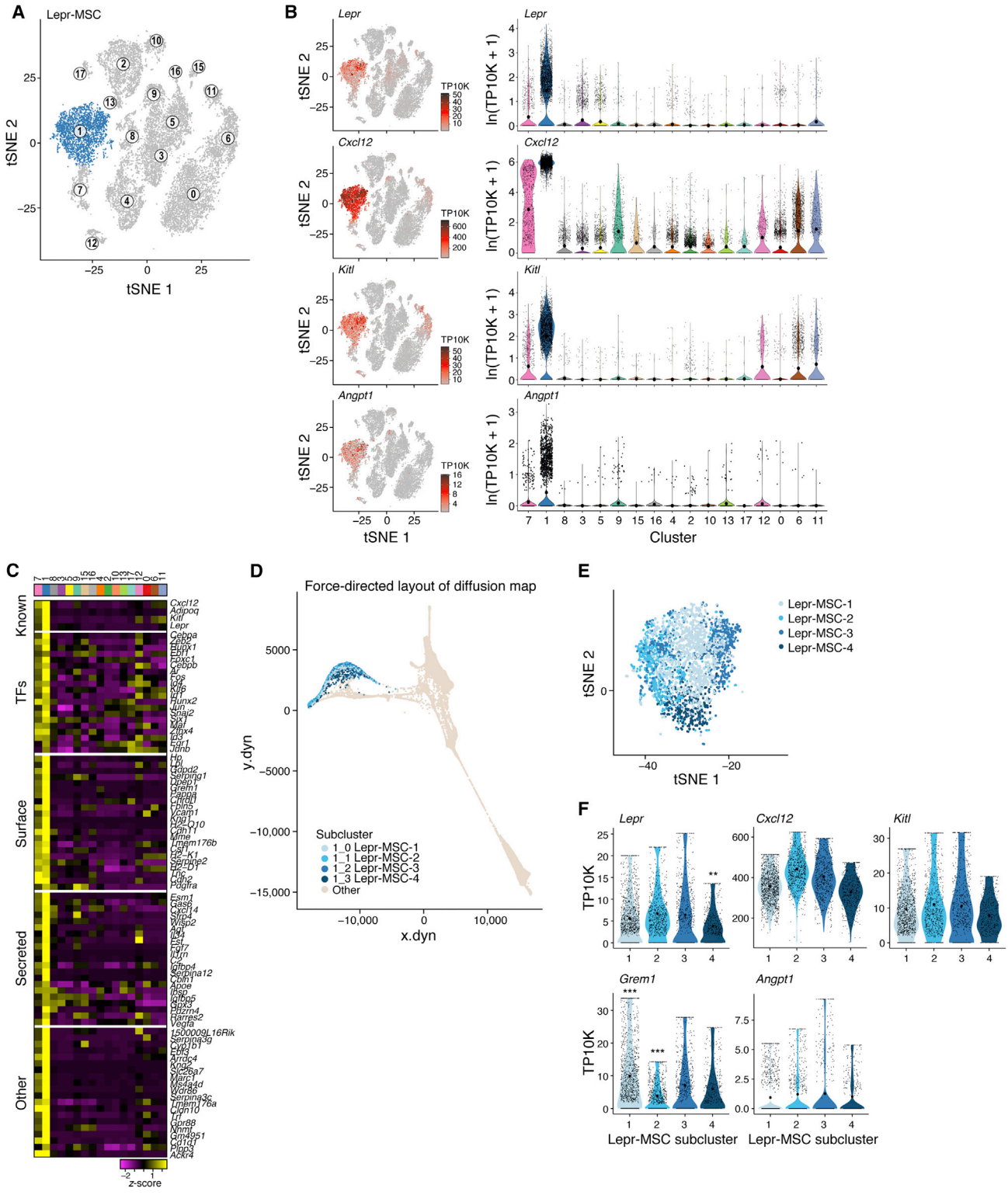

Figure 2. Four Subsets of HSC Regulator-Producing Lepr-MSCs Form a Differentiation Continuum

(A–C) Signature genes for Lepr-MSCs in the stroma atlas.

(A and B) t-SNE of Figure 1B colored by cluster-1 membership (A) or by expression (color bar, TP10K) of key MSC marker genes (B, left), along with the corresponding distributions of expression levels (ln(TP10K+1), y axis) across clusters of Figure 1B (x axis) (B, right).

(legend continued on next page)

Within Lepr-MSCs, we distinguished four major subsets (Lepr-MSC-1–4) by subclustering and diffusion trajectory analysis (Angerer et al., 2016) (Figures 2D, 2E, S2D, and S2E). While *Kitl* and *Angpt1* were comparably expressed in all four subsets, they were distinguished by the expression of *Cxcl12*, *Lepr*, *Grem1*, and multiple other genes (Figures 2F and S2E). In particular, one subset (Lepr-MSC-4) had significantly higher expression of the key functional OLC-specification genes Sp7 (osterix) and *Alpl* (Huang et al., 2007; Nakashima et al., 2002), while the OLC-specification gene *Runx2* showed no difference between the subclusters (Figures S2E and S2F), suggesting differentiation toward the osteoblastic lineage, supported by the continuous transition inferred between cells from the Lepr-MSC and OLC-1 clusters in differentiation trajectories (Figures 1G and 1H). Indeed, OLCs that include osteoprogenitors and mature osteoblasts can be derived from MSCs (Park et al., 2012; Worthley et al., 2015; Zhou et al., 2014a).

Inferred Lineage Relations Suggest Two OLC Subsets of Different Differentiation Origins and Distinct Hematopoietic Support Potential

To further analyze osteolineage differentiation, we focused on Lepr-MSC-4, along with cluster 7 (OLC-1) and 8 (OLC-2) (Figure 3A) that expressed the osteoblast maturation marker *Bglap* (Figures 3B and S3A) (Delmas et al., 1986) and formed a continuum in the diffusion map (Figure 1H). All three clusters differentially expressed *Runx2*, the master regulator transcription factor (TF) controlling the commitment of MSCs to OLCs (Huang et al., 2007), and both OLC-1 and OLC-2 further expressed *Sp7*, its downstream target TF, which together are required for early and late osteolineage differentiation (Figures 3B, 3C, and S3A). Furthermore, *Bglap* was expressed in a subset of the clusters, along with other osteoblastic maturation makers (*Alpl*, *Col1a1*, *Spp1*, and *Pth1r*) (Huang et al., 2007) (Figures 3B, 3C, and S3B).

Whereas Lepr-MSC-4 consisted of putative committed osteolineage MSCs, the cells in OLC-1 spanned a continuum of osteoblastic states in the diffusion map (Figures 3D and 3E) and differential gene expression (Figure S3C) analyses, including, in order: (1) early osteoprogenitors that were in a cell transition-state from Lepr-MSC-4 (Figures 2E, 3D, and 3E), expressing *Runx2*, *Sp7*, *Grem1*, *Lepr*, *Cxcl12*, and *Kitl* (Figures 3F, 3G, and S3C) but not osteoblast maturation markers (*Bglap* and *Col1a1*) (Figure 3H); (2) preosteoblasts (e.g., late osteoprogenitors), highly expressing the osteoprogenitor marker CD200 (Abdallah et al., 2015; Chan et al., 2015), and *Spp1* (Figure 3I), a marker of later stages of osteoblastic differentiation (Huang et al., 2007) but lowly expressing osteoblast maturation markers (Figure 3H); and (3) mature osteoblasts expressing *Bglap* and *Col1a1* (Figure 3H). In addition, the subcluster included (4) putative chondrocytes expressing low levels of *Sox9*, a TF essential for chondrocyte differentiation (Foster et al., 1994; Wagner et al., 1994), and *Acan*, a chondrocyte marker gene (Doege et al., 1991) (Figure 3J).

Remarkably, the OLC-2 (mostly bone origin) (Figure 1B, inset) cells highlighted a distinct subset of OLCs from those found in a continuum from Lepr-MSC-4. Along the continuum spanned by OLC-2 cells (Figures 3D, 3K, and S3D; Table S2) we observed: (1) osteoprogenitors (8_3), expressing *Runx2*, *Sp7*, *Grem1*, and *Mmp13*, the matrix metalloproteinase that regulates the calcification and degradation of cartilage during the endochondral ossification process (Nishimura et al., 2012) (Figures 3L and S3E), but low levels of *Bglap* and *Sox9* (Figures 3M and S3E); (2) osteoblasts (8_2) expressing OLC markers (*Runx2*, Sp7, *Spp1*, *Bglap*, and *Pth1r*) (Figures 3L, 3M, and S3E); and (3) osteo and/or chondrocytes (8_0, 8_1, 8_4, and 8_5) that appeared to be in the process of being ossified into bone (Yang et al., 2014; Zhou et al., 2014b). Notably, only OLC-1 cells expressed key hematopoietic regulatory cytokines (albeit 8_3 in OLC-2 expressed relatively low levels *Cxcl12*) (Figure 3M) suggesting that there were two OLC subsets of distinct differentiation origins and with distinct hematopoietic support potential.

Characterization of Chondrocyte Cell Differentiation

We next examined the differentiation of chondrocytes. Cells in five clusters (clusters 2, 4, 10, 13, 17) all expressed the chondrocyte lineage genes *Sox9*, *Acan*, and *Col2a1* (Figures 4A and 4B), formed a sequence in the overall diffusion map (Figure 4C), and distinguished (1) proliferating and resting chondrocytes (cluster 10) expressing *Col2a1* (Inada et al., 1999) (Figures 4A, 4B, and S1I), (2) prehypertrophic chondrocytes that started the maturation process (clusters 2 and 17), co-expressing *Ihh*, *Pth1r* (Vortkamp et al., 1996), and *Mef2c* (Arnold et al., 2007) (Figures 4A and S4A–S4C), (3) hypertrophic chondrocytes (cluster 2) co-expressing *Runx2*, *Ihh*, *Mef2c*, and *Col10a1* (Figures 4A and S4A–S4C) (Arnold et al., 2007), as well as (4) putative chondrocyte progenitor cells (cluster 4) that were in transition into OLC-2 (Figures 1H and 4C) expressing *Grem1* (Figure S4B), OLC markers (*Runx2*, *Sp7*, *Alpl*, *Spp1*) (Figures 3B and S3B), and chondrocyte markers (*Sox9*, *Acan*) (Figure 4B).

A Fibroblast Subset Expresses Hematopoietic Niche Regulators

Fibroblasts are cells of mesenchymal origin that are ubiquitous in the bone marrow and consist of phenotypically and functionally distinct subpopulations (Kalluri, 2016). Due to the paucity of distinctive markers and similar morphology and phenotypes, they are commonly confounded in the bone marrow with MSCs

(C) Expression (row-wide *Z* score of ln of average TP10K) of top differentially expressed genes (rows) in the cells of each cluster (columns) (color bar, top, as in Figure 1B), ordered by five gene categories (labels on left).

(D–F) Four major Lepr-MSC subclusters span a differentiation continuum.

(D and E) Continuous transition across the subclusters (D). Four subclusters colored on the FLE of the diffusion map from Figure 1H (E) or on a zoom-in to the Lepr-MSC cluster in (A).

(F) Distributions of expression levels (TP10K, y axis, censored scale) for select marker genes across the 4 subclusters. Stars for significant differential expression of select genes.

See also Figure S2 and Tables S1 and S2.

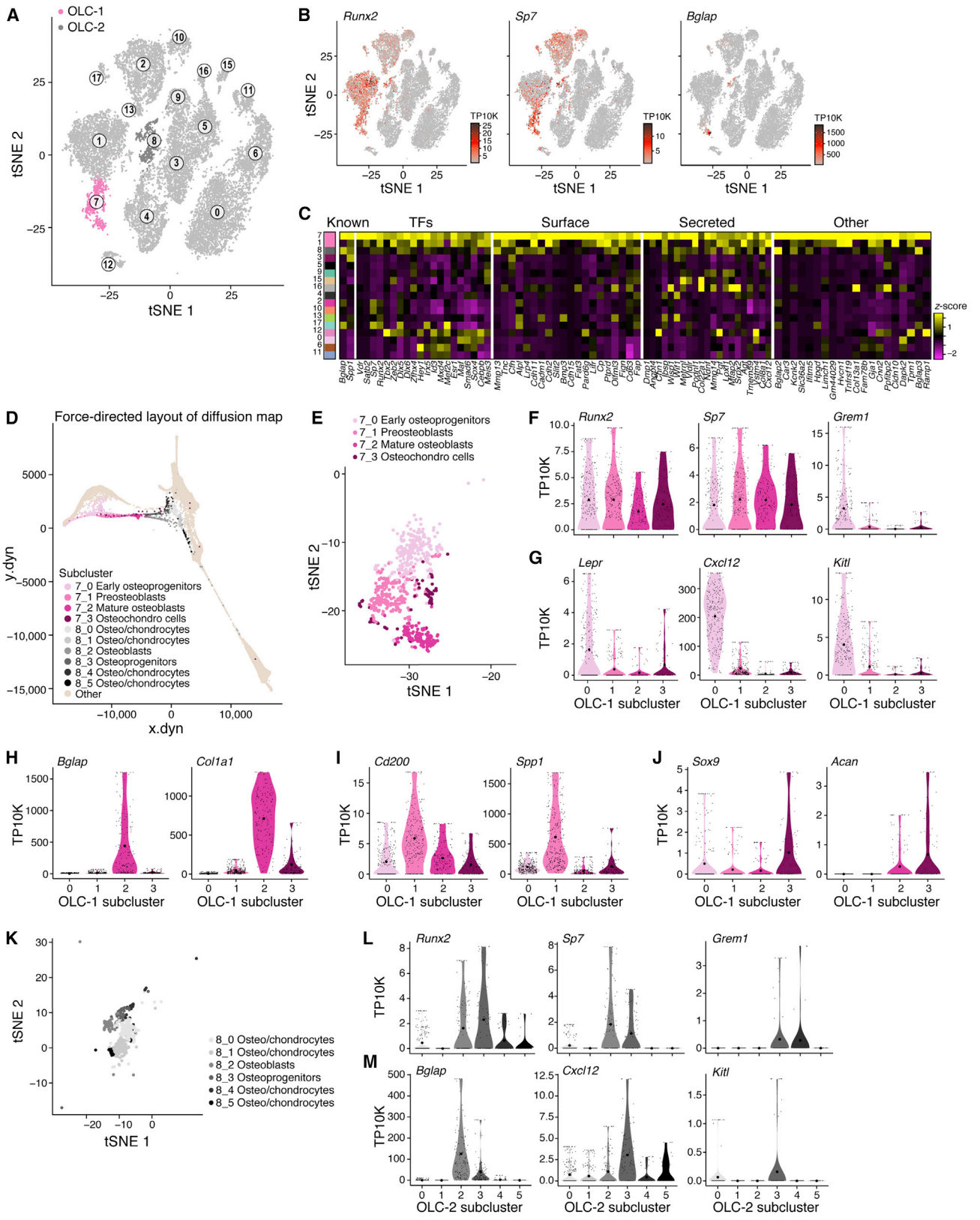

(legend on next page)

and pericytes limiting the accuracy of functional studies (Soundararajan and Kannan, 2018).

Five fibroblasts clusters (3, 5, 9, 15, 16) all highly expressed the fibroblast specific genes fibronectin-1 (*Fn1*), *S100a4*, decorin (*Dcn*), and semaphorin-3C (*Sema3c*) (Figures 4D, 4E, and S4D) lowly expressed the chondrocyte genes *Sox9*, *Acan*, and *Col2a1* (Kalluri, 2016) (Figure 4B), and were distinguishable from both Lepr-MSCs and pericytes.

Fibroblast-1 s (cluster 9) and fibroblast-2 s (cluster 15) cells expressed the progenitor marker *Cd34* (Figure S1G) and MSC markers (*Ly6a*, *Pdgfra*, *Thy1*, and *Cd44*) (Figures S4D and S4E), but not BMEC or pericytes genes (*Cdh5*, *Acta2*) (Figure 1C), suggesting these fibroblasts are MSC-like. Fibroblast-1 s also expressed *Cxcl12* and *Angpt1* (Figures 2B and 4G) indicating a possible niche regulatory function that resembles CAFs that facilitate cancer growth and metastasis (Ahirwar et al., 2018; Costa et al., 2018).

Fibroblast-3 (cluster 16), fibroblast-4 (cluster 3), and fibroblast-5 (cluster 5) were related to tendon and/or ligament cells. They co-expressed *Sox9* (Figure 4B) and the TF scleraxis (*Scx*) (Figure S4F) that regulate differentiation of tenocytes and ligamentocytes (Sugimoto et al., 2013). Fibroblast-4 and fibroblast-5 s further expressed key bone and cartilage genes including the *Spp1* (Figure S3B) and the chondrocyte genes *Nt5e*, *Cspg4* (Figures S2A and S2B), and *Cilp* (Figure S4F). The three clusters formed a continuum from fibroblast-3 s to fibroblast-4 s and fibroblast-5 s (Figure 4F). Thus, fibroblast-3 s may be tenocyte progenitors (Sugimoto et al., 2013), whereas fibroblast-4 s and fibroblast-5 s may consist of tendon and/or ligament cells (Sugimoto et al., 2013).

Arterial BMECs Express Higher Levels of Niche Factors Compared to Sinusoidal and Arteriolar Vascular Cells

We identified three BMEC subsets each supported by distinct differentially expressed genes (Figures 5A, 5B and S5B; Table S1): cluster 0 consisted of putative sinusoidal BMECs, cluster 6 of cells from arterioles and/or capillaries, and cluster 11 containing BMECs from endosteal and bone marrow arteries. All subsets were related along a continuum (Figure 5C) and expressed known markers of endothelial cells—*Pecam1*, *Cdh5*, Cd34, *Kdr*, and *Emcn* (Rafii et al., 2016) (Figures 5B and 5D). We annotated cluster 0 and 6 cells as sinusoidal and arteriolar BMECs (sBMECs and aBMECs), respectively. Cluster 0 cells had high expression of *Flt4* (Vegfr-3) and low expression of *Ly6a* (Sca-1), while cluster 6 cells had the opposite pattern (Figure S5A). This was consistent with previous reports that sBMECs are Vegfr-3^{+}/Sca-1^{-} while arteriolar cells are Vegfr-3^{-}/Sca-1^{+} (Hooper et al., 2009; Itkin et al., 2016). Bone-marrow imaging was used to determine whether cluster 11 is a subset of aBMECs or sBMCEs. Vwf, expressed exclusively but heterogeneously in cluster 11, stained endosteal and some bone marrow arteries but not sinusoids (Figures 5E, 5F, and S5C) indicating these cells are a subset of aBMECs. *Cd34* has been previously associated with aBMECs, not sinusoids, and we noted gene expression in clusters 6 and 11, not cluster 0 (Coutu et al., 2017). In contrast, *Il6st*, predominantly expressed in cluster 0 and not cluster 6 nor 11 (Figures 5F and S5B), exclusively stained bone marrow sinusoids by bone marrow imaging (Figure 5E). Therefore, cluster 11 is a subset of aBMECs.

The three subsets expressed different ligands and secreted factors (Figure 5B). All three expressed the endothelial tyrosine kinase receptor, Tie2 (*Tek*), for angiopoietin ligands (Figures 5G and S5D). However, *Kitl* and *Cxcl12* were most abundant in aBMECs, and *Kitl* most highly expressed by cluster 11 when compared with cluster 6 (Wilcoxon rank-sum test p value 6.9×10^{-5} and 35% higher average expression per cluster), while sBMECs expressed vastly smaller quantities of either factor (Figure 5G). Differential expression analysis comparing differences between both aBMEC clusters revealed a number of genes characterizing both clusters (Figure S5E; Table S3), suggesting that arterial BMEC may be a distinctively relevant subpopulation within BMECs, that regulates HSC function as has been previously proposed (Ding et al., 2012; Xu et al., 2018).

Pericyte Subpopulations Vary in Hematopoietic Regulatory Gene Expression

NG2^{+} and Nestin^{+} perivascular MSCs have been proposed as critical regulators of HSC function through production of *Cxcl12* and *Kitl* (Kunisaki et al., 2013; Méndez-Ferrer et al., 2010). Notably, under homeostasis, HSCs reside in perisinusoidal or periarteriolar locations predominantly found in close proximity to Lepr-Cre^{+} cells, also shown to produce *Cxcl12* and *Kitl* (Acar et al., 2015; Ding et al., 2012; Morrison and Scadden, 2014). However, determining whether NG2^{+} and Nestin^{+} perivascular MSCs share developmental origins and functional properties with perivascular Lepr-Cre^{+} cells has been challenging because there is currently no single marker that separates them (Armulik et al., 2011).

We annotated a distinct cluster of perivascular mesenchymal stromal cells and pericytes (cluster 12; hereafter referred to as

Figure 3. Two OLC Subsets of Distinct Differentiation Origins and Hematopoietic Support Potential

(A–C) Two OLC subsets.

(A and B) t-SNE of Figure 1B colored by cluster 7 (OLC-1) and cluster 8 (OLC-2) membership (A), or by expression (color bar, TP10K) of key OLC marker genes (B).

(C) Expression (column-wide *Z* score of ln of average TP10K) of top differentially expressed genes (rows) ordered by four gene categories (labels on top) in the cells of each cluster (columns, color bar, left, as in Figure 1B).

(D) Continuous transition across the subclusters. OLC-1 and OLC-2 subclusters color coded on the FLE of the diffusion map from Figure 1H.

(E–J) OLC-1 subsets.

(E) A zoom-in to OLC-1 in (A) labeled by four major subclusters and annotated post hoc (legend).

(F–J) Distributions of expression levels (TP10K, y axis, censored scale) for select marker genes across the OLC-1 subclusters.

(K–M) OLC-2 subsets.

(K) A zoom-in to OLC-2 in (A) labeled by six subclusters and annotated post hoc (legend).

(L and M) Distributions of expression levels (TP10K, y axis, censored scale) for select marker genes across the OLC-2 subclusters.

See also Figure S3 and Tables S1 and S2.

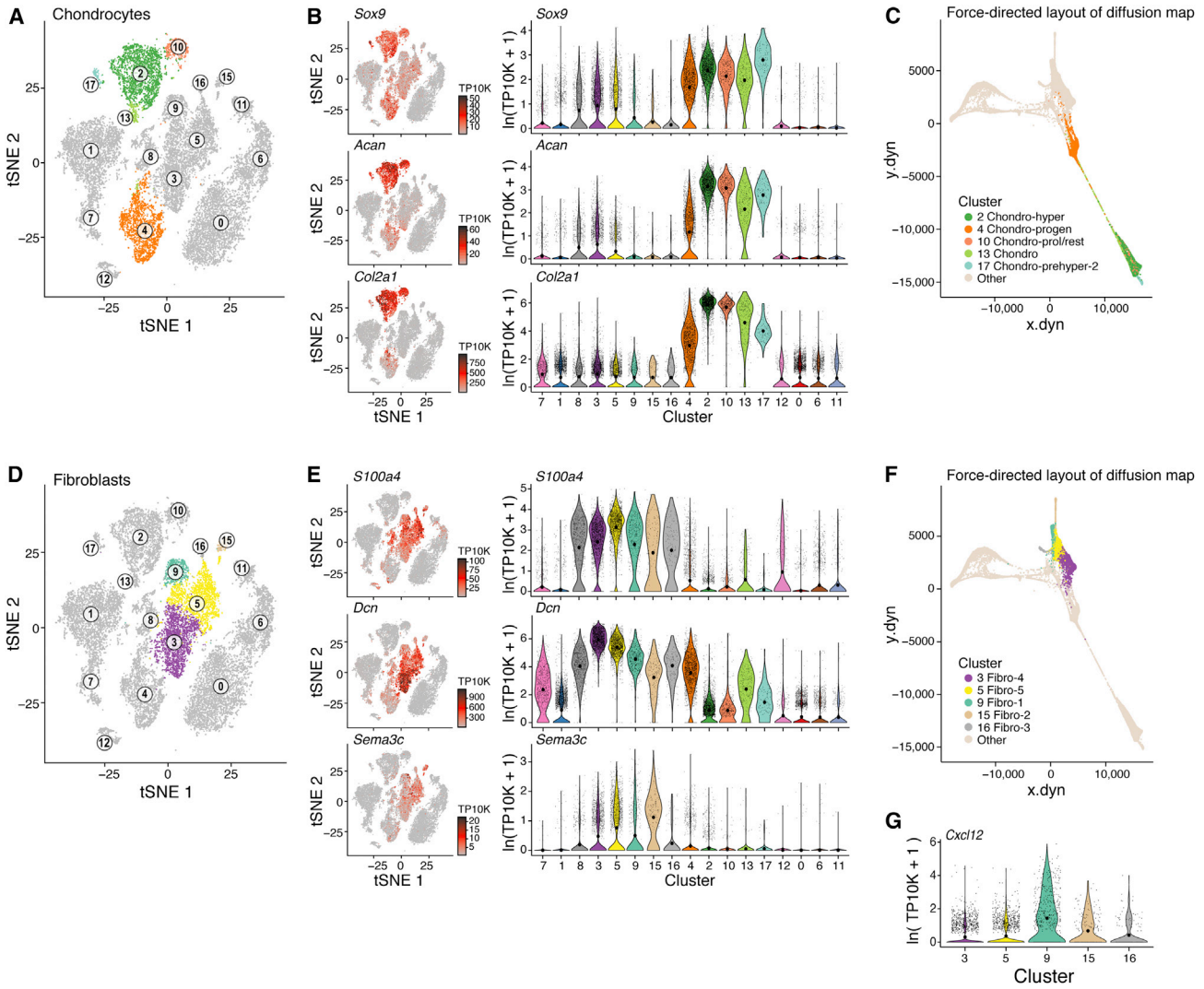

Figure 4. Chondrocyte and Fibroblasts Subsets Highlight Differentiation Paths and Hematopoiesis Support, Respectively

(A–C) Subsets across chondrocyte differentiation.

(A and B) Signature genes for chondroid subsets. t-SNE of Figure 1B colored by membership in five chondroid clusters (A), or by expression (color bar, TP10K) of key marker genes (B, left), along with the distributions of expression levels (ln(TP10K+1), y axis) for the same genes across clusters of Figure 1B (x axis) (B, right).

(C) Continuous transition across the chondroid subclusters. The five subclusters colored on the FLE of the diffusion map from Figure 1H.

(D–F) Fibroblast subsets.

(D and E) Signature genes for fibroblast subsets. t-SNE of Figure 1B colored by membership in five fibroblast clusters (D), or by expression (color bar, TP10K) of key marker genes (E, left), along with the distributions of expression levels (ln(TP10K+1), y axis) for the same genes across the clusters of Figure 1B (x axis) (B, right).

(F) Relations between the fibroblast subclusters. The clusters colored on the FLE of the diffusion map from Figure 1H.

(G) Distribution of *Cxcl12* expression level (ln(TP10K+1), y axis) across the fibroblast clusters (x axis).

See also Figure S4 and Table S1.

Pericytes), by the co-expression of the classical MSC markers *Nes*, NG2 (*Cspg4*), and the pericytes markers *Acta2*, *Myh11*, and *Mcam* (Armulik et al., 2011) (Figures 6A–6C and S6A). The pericytes differentially expressed *Jag1*, the Notch signaling ligand, and *Il-6*, both implicated in promoting HSC maintenance (Bernad et al., 1994; Calvi et al., 2003) (Figure S6C). Notably, cells in this cluster expressed only very low levels of *Lepr*, in contrast to the high expression of *Lepr* in Lepr-MSCs (Figures 2B and 2C). Thus, pericytes and Lepr-MSCs were clearly distinguishable.

Within the pericytes, we identified three subsets (Figures 6D and S6B; Table S2). Pericyte-1 cells, distinguished by relatively higher expression of *Cdh2*, *Lepr*, and specific expression of MSC marker *Ngfr*, expressed *Kitl* most abundantly with low levels of *Cxcl12* (Figures 6E and 6F). Conversely, pericyte-3 expressed *Cxcl12* with minimal *Kitl* and pericyte-2 expressed low

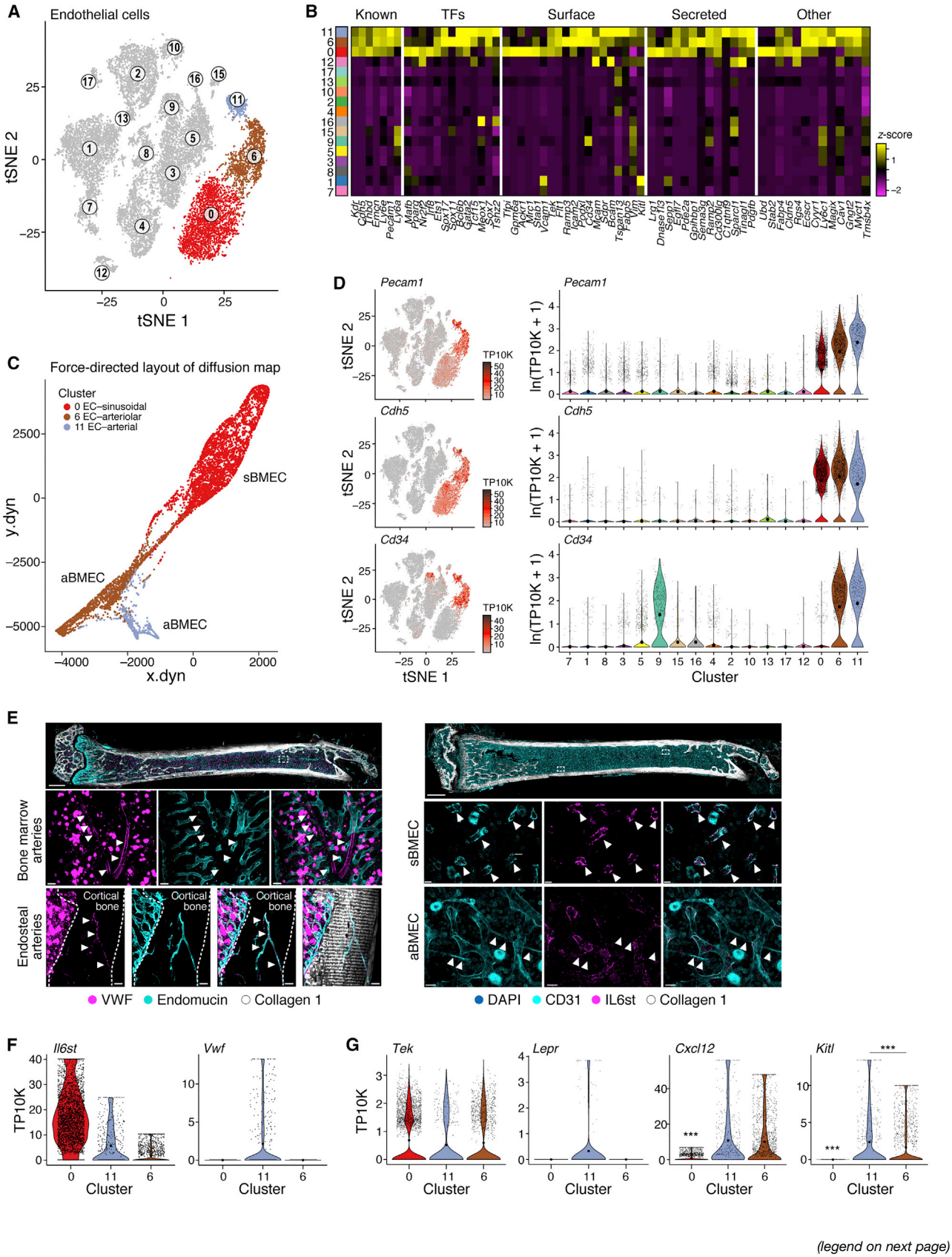

(legend on next page)

levels of both, suggesting a possible distinction in HSC support. Pericyte-2 and pericyte-3 had molecular features similar to previously reported periarteriolar cells (NG2-CreER/Nes-GFP^{high}) (Coutu et al., 2017; Kunisaki et al., 2013) and perisinusoidal cells (Nes-GFP^{+}) (Méndez-Ferrer et al., 2010) respectively. Unlike Lepr-MSCs, none of the pericyte subsets expressed high levels of both *Cxcl12 and Kitl* (Figures 2F, 6E, and 6F). Therefore, while Lepr-MSC, NG2^{+} and Nes^{+} cells have each been defined as HSC niche cells, they are molecularly distinct.

Systemic Survey of Changes in Bone Marrow Stromal Cells Induced by Emerging Primary Leukemia

Several bone marrow stromal cell populations that regulate hematopoiesis can, when perturbed, lead to niche-initiated myelodysplasia or leukemia in animal models (Arranz et al., 2014; Dong et al., 2016; Kode et al., 2014; Raaijmakers et al., 2010). Moreover, myeloid malignancies can remodel their niche to support malignant growth (Hanoun et al., 2014; Schepers et al., 2013; Schmidt et al., 2011).

To comprehensively assess changes in the stroma during malignant growth, we compared (Corral et al., 1996) stromal cell scRNA-seq from mice with normal or MLL-AF9 knockin bone marrow transplanted 6–10 months before analysis (Figures 7A, 7B, and S7A–S7D; Table S1).

Remodeling of Bone Marrow Stromal Cell Proportions in Leukemia

We detected significant changes in the proportions of key subsets in leukemia. These often reflected coupled effects in OLCs (increase in OLC-1, reduction in OLC-2), BMECs (reduction in sBMECs, increase in cluster 6 aBMECs), chondrocytes (increase in cluster 2, decrease in 4), and fibroblasts (decrease in fibroblast-5 s, increase in fibroblast-2 s) (Figures 7C and S7E).

The shift in OLCs was consistent with previous studies of leukemia, where OLC lineage dysfunction is caused by leukemia cells and favorable for their growth (Duarte et al., 2018; Frisch et al., 2012; Hawkins et al., 2016; Krevvata et al., 2014; Schepers et al., 2013). Moreover, proportions also varied within the OLC-1 subset with a significant increase in preosteoblasts (subcluster 1), but not in other cells (Figure 7D). While the overall proportion of Lepr-MSCs was unchanged, the relative proportions within were impacted by leukemia with significant increase in subcluster 2 and a concomitant reduction in subcluster 3 and 4 (committed osteolineage Lepr-MSCs) (Figures 7D and S7E). Overall, the concomitant decrease in committed osteolineage Lepr-MSCs and increase in preosteoblasts suggests that leukemia induced a block in osteolineage development (Hanoun et al., 2014; Kumar et al., 2018). The changes observed in Lepr-MSCs and OLCs, as well as BMECs, were consistent with the reported abnormalities seen in AML patients where leukemia induces vasculature remodeling that is accompanied by reduced osteocalcin (*Bglap*) serum levels, growth deficiency, and impaired osteogenesis (Duarte et al., 2018; Geyh et al., 2016; Kumar et al., 2018; Passaro et al., 2017).

Leukemia Compromises Osteogenic and Adipogenic Differentiation Pathways in Lepr-MSCs and OLCs

Analyzing changes in intrinsic gene programs within each cluster highlighted blunted adipogenic and osteogenic differentiation programs in Lepr-MSCs and OLCs (Figures S7F and S7G; Table S4). Cells in both clusters downregulated *Grem1* (Worthley et al., 2015) across all Lepr-MSC subclusters and in early osteoprogenitors (subcluster 0) (Figure 7E) as well as the BMP pathway, including *Bmp4* (GSEA) (Subramanian et al., 2005) (GSEA q-value [qval] = 0.027, Table S4) (Wozney et al., 1988) and the early OLC-specification gene *Sp7* (Figure 7F). Mature osteoblasts within OLCs further downregulated *Runx2*, an early marker of osteogenesis, and *Bglap1–3*, late markers of osteogenesis (Lee et al., 2007) (Figures 7F and S7F). Lepr-MSC cells further downregulated *Adipoq* (Figures 7F and S7F) (Bauche et al., 2007) and other genes in the white adipocyte differentiation (GSEA qval = 0.029, Table S4) and the PPAR signaling pathways (GSEA qval = 0.022, Table S4) (Tontonoz et al., 1994). This was consistent with reports that AML induces a compromised adipocytic niche that leads to imbalanced stem and progenitor regulation and is not favorable for normal blood cell production (Boyd et al., 2017). Furthermore, *Wisp2*, which has been implicated in restricting MSCs to an undifferentiated state (Grünberg et al., 2014; Hammarstedt et al., 2013) was upregulated in all Lepr-MSC subsets and OLC progenitors (subclusters 0 and 1) (Figures S7F and S7I) further supporting compromised differentiation of Lepr-MSCs and OLCs. Conversely, key genes that inhibit bone formation and calcification were induced in Lepr-MSCs and OLCs (and others) including *Mgp* (inhibits calcification) (Luo et al., 1997),

Figure 5. Arterial BMECs Express Higher Levels of Niche Factors Compared to Sinusoidal and Arteriolar Vascular BMECs

(A and B) Three BMEC subsets.

(A and B) t-SNE of Figure 1B colored by membership in three BMEC clusters (A), or expression (column-wide *Z* score of ln of average TP10K) of top differentially expressed genes (columns) ordered by five gene categories (labels on top) in the cells of each cluster (rows, color bar, left, as in Figure 1B) (B).

(C) Continuous transition across the subclusters. FLE of a diffusion map of BMECs, color coded by cluster membership.

(D) Expression (color bar, TP10K) of key marker genes (right), along with the distributions of expression levels (ln(TP10K+1), y axis) for the same genes across clusters of Figure 1B (x axis) (left).

(E) Left: VWF expression in endosteal arteries, but not sinusoids. Left top: high magnification images of femoral diaphysis showing VWF expression by arteries (white arrowheads) in addition to megakaryocytes, but not endomucin-expressing sinusoids or central sinus (left bottom). Endosteal arteries (white arrowheads) marked by both VWF and endomucin. Bone surface is marked by Col.1 expression. Scale bars are 100 μm (full bone) 50 μm (inserts). Right: IL6st expression in venous, but not arteriolar endothelium. Full-bone imaging of femoral sections showing sinusoidal endothelium expressing both CD31 and IL6st (right top), while arteriolar endothelium is only expressing CD31. Bone surface is marked by Col.1 expression. Scale bars are 700 μm (full bone), 15 μm (mid panel), and 20 μm (low panel).

(F and G) Key marker genes. Distributions of expression levels (TP10K, y axis) for select genes across the three clusters (x axis). Stars for significant differential expression of select genes.

See also Figure S5 and Tables S1 and S3.

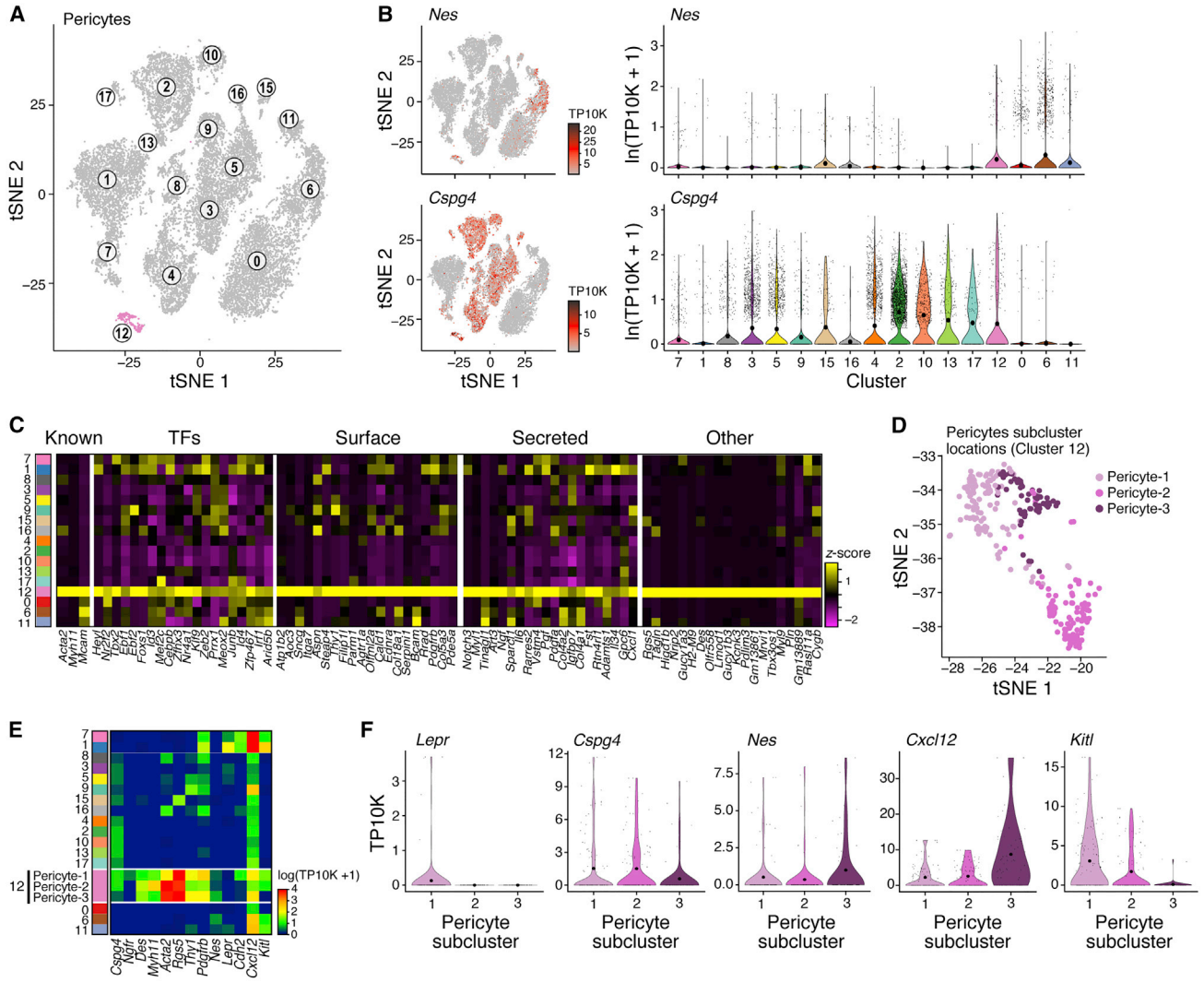

Figure 6. Three Distinct Subpopulations of Pericytes that Vary in Hematopoietic Regulatory Gene Expression

(A–C) Signature genes for Pericytes in the stroma atlas.

(A and B) t-SNE of Figure 1B colored by cluster-12 membership (A), or by expression (color bar, TP10K) of key pericyte marker genes (B, left), along with the distributions of expression levels (ln(TP10K+1), y axis) for the same genes across the clusters of Figure 1B (x axis) (B, right).

(C) Expression (column-wide *Z* score of ln of average TP10K) of top differentially expressed genes (columns) in the cells of each cluster (rows) (color bar, left, as in Figure 1B), ordered by five gene categories (labels on top).

(D) Pericyte subclusters color coded on the zoom-in of to the pericyte cluster from (A).

(E) Average expression (ln(TP10K+1)) of select HSC niche genes (x axis) in clusters of Figure 1B (y axis). Three pericyte subclusters indicated.

(F) Distributions of expression levels (TP10K, y axis, censored scale) for select marker genes across the subclusters.

See also Figure S6 and Tables S1 and S2.

Igbfp5 and *Igfbp3* (negative regulators on bone formation) (Kanatani et al., 2000; Silha et al., 2003), and genes in the ECM degradation pathway (GSEA qval = 0.04, Table S4) including *Mmp2*, *Mmp11* and *Mmp13* (Figures 7F and S7F). Taken together, these data are consistent with AML inducing alterations that affect bone formation and breakdown.

The cell profiles further support a model where hypoxia contributes to the undifferentiated state of the MSCs and OLCs (Kim et al., 2009). Hypoxia pathway genes (GSEA qval = 0.004, Table S4) were induced in MSCs and OLCs, including the key regulator Hif-2a (*Epas1*), but not *Hif-1a* (Figures 7G, S7H, and S7J), consistent with reports that suppression of bone formation and osteoblast activity is directly linked to Hif-2a and not Hif-1a (Rauner et al., 2016). Notably, the *Wisp2* promoter is regulated by Hif-2a (Fuady et al., 2014).

Leukemia Broadly Impairs Normal Hematopoiesis-Regulatory Gene Expression

The changes in the stroma may contribute to altered support of normal blood cell growth through deregulation of the expression

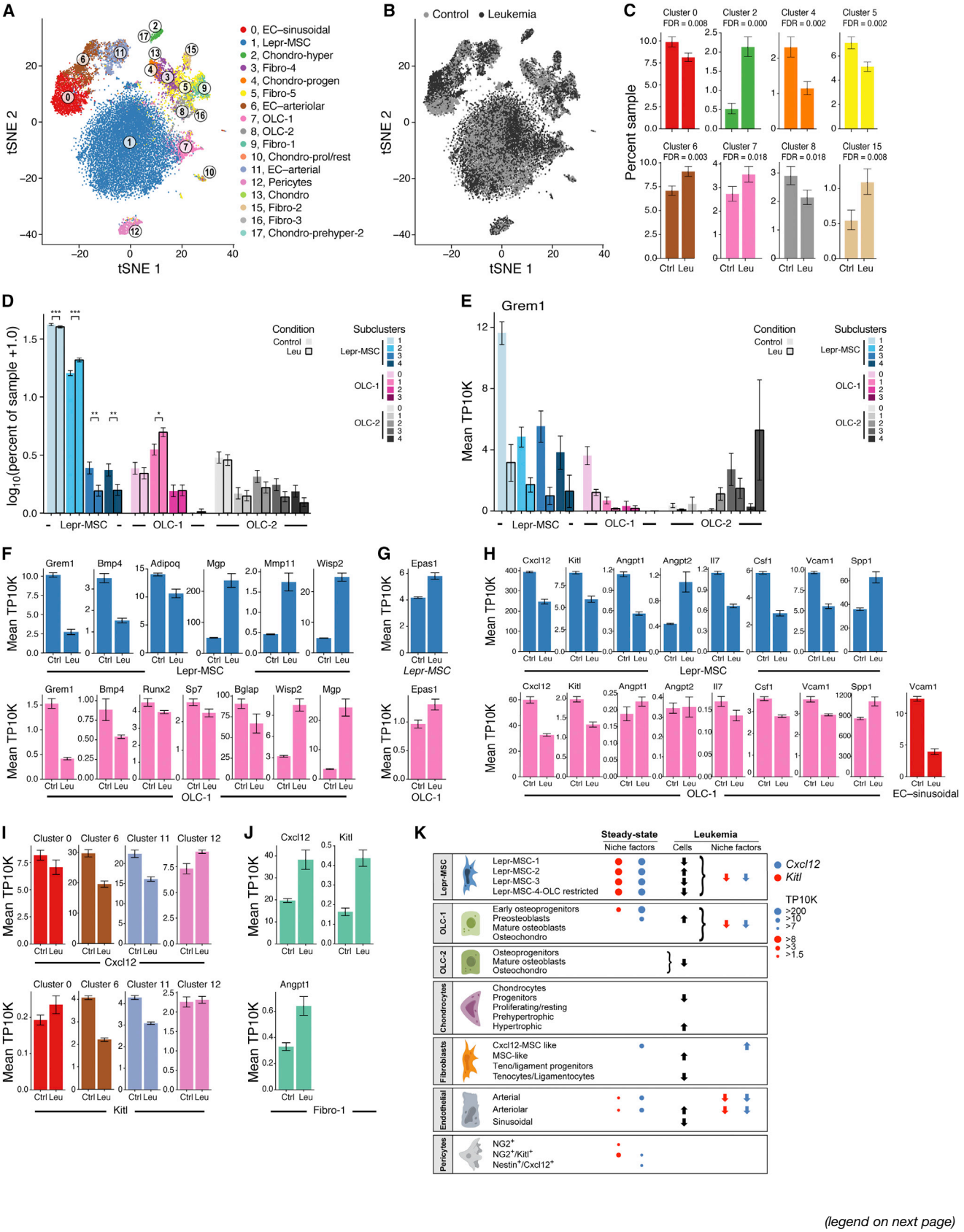

(legend on next page)

of key HSC niche factors, especially *Cxcl12* and *Kitl* across Lepr-MSCs, clusters 6 and 11 aBMECs, and the earliest OLCs (subcluster 0) (Figures 7H and 7I); conversely, *Cxcl12*, *Kitl*, and *Angpt1* were upregulated in fibroblast-1 s (Figure 7J). These findings are consistent with prior observations of AML reducing HSC persistence and localization to the bone marrow (Zhang et al., 2012), and Cxcl12-secreting-CAFs (similar to fibroblast-1 s) are associated with a cancer-promoting phenotype in breast cancer (Ahirwar et al., 2018; Costa et al., 2018).

Among other factors, *Spp1*, a negative regulator of HSC pool size (Stier et al., 2005) and HSC proliferation (Nilsson et al., 2005), which is correlated with poor prognosis in AML patients (Chen et al., 2017), was upregulated in Lepr-MSCs, OLCs, BMECs, fibroblasts, and pericytes (Figures 7H and S7F). Lepr-MSCs downregulated other HSC niche factors including *Angpt1*, an agonist of *Tek* receptor expressed on BMECs and HSCs (Arai et al., 2004) (and upregulated its antagonist *Angpt2*) (Gomei et al., 2010), factors that promote lymphoid (*Il7*) (Muegge et al., 1993; Namen et al., 1988) or myeloid (*Csf1*) differentiation (Mossadegh-Keller et al., 2013), and *Vcam1*, a regulator of HSC homing to bone marrow (Papayannopoulou et al., 1995) (Figure 7H). Thus, the osteogenic differentiation block induced by leukemia in Lepr-MSCs and OLCs was further accompanied by a loss of HSC niche factor production by multiple cell types.

DISCUSSION

While it is now well-appreciated that non-parenchymal cells in the stroma of a tissue play key physiological roles in forming niche cells (Calvi et al., 2003; Zhang et al., 2003), the full repertoire of cells that comprise stroma has remained elusive in all complex adult tissues, including the bone marrow. Here, we systematically characterize the stroma of the mouse bone and bone marrow into six broad cell types with 17 cell subsets, with discrete distinctions, differentiation continuums, and HSC niche regulatory function often disrupted by the emergence of leukemia (Figure 7K). Note that a complementary analysis of bone marrow stroma using scRNA-seq has been published after this manuscript was accepted in principle (Tikhonova et al., 2019), which focused on several cell subpopulations pre-sorted by pre-defined markers and on a stress model.

These findings provide a clear set of definitions and tools, including refined understanding of the relation between markers and cell types (and their limitations), clarify prior controversies, and lead to several unexpected observations. Here, we highlight some of these key findings.

First, OLCs segregated into two subsets that appear to arise from distinct lineage trajectories. Only one of these, which emerges from Lepr-MSCs, expresses high HSC regulatory genes and does so at the early osteoprogenitor stage of development.

Second, one of the five fibroblasts subsets we identified expressed *Cxcl12*. Cxcl12-expressing fibroblasts have been implicated in aggressive solid tumors (Ahirwar et al., 2018; Costa et al., 2018). We thus hypothesize that they may participate in bone metastases; future studies can test this possibility.

Third, BMECs consisted of a distinctive artery subset that was enriched for expression of hematopoietic regulators. This cell population was apparent in a peri-endosteal location and bone marrow and was in marked contrast to the large sinusoidal endothelium subset that minimally expressed the HSC niche factors, Cxcl12 and Kitl, despite prior reports that peri-sinusoidal positioning of HSC is common (Acar et al., 2015).

Fourth, we clarified that Lepr^{+} cells are common across multiple cell types, including osteolineage, endothelial, pericyte, and fibroblastic cells. Thus, the use of Lepr-driven Cre to alter particular genes could impact their expression across many cell types and must be interpreted with extreme care, especially where Lepr-Cre is expressed throughout development, as commonly done to date (Zhou et al., 2014a). We further showed that there was discordant expression of *Cxcl12* and *Kitl* among pericyte subpopulations that segregated with low level *Lepr*, NG2 (*Cspg4*), and *Nes* expression. Future studies can assess if these reflect functional distinctions in hematopoietic support, and how this subpopulation tracks with periarteriolar, quiescent HSCs (Kunisaki et al., 2013).

Finally, the presence of AML distorted the stromal compartment in select and specific ways. Osteogenic differentiation blockade occurs in Lepr-MSCs and OLCs, is accompanied by a cell intrinsic bone remodeling phenotype, and disturbed production of hematopoietic regulatory factors that affect normal hematopoiesis. While most studies show that osteoblast numbers are either reduced (Frisch et al., 2012; Krevvata et al., 2014; Kumar et al., 2018) or increased (Hanoun et al., 2014; Schepers et al., 2013), depending on type of leukemia model used, our study supports a loss of bone maturation phenotype and function. A parenchymal tumor affecting the maturation of tissue stromal cells does suggest a distinct type of cross-interaction between emerging cancer cells and their mesenchymal neighbors. It may be that differentiation blockade is not restricted

Figure 7. Remodeling of the Bone Marrow Stroma in Leukemia

(A and B) Census of the leukemic bone marrow stroma. t-SNE of 23,004 cells (dots) from mice transplanted with control (n = 5, 12,456 cells) or leukemia allele bearing (n = 4, 10,548 cells) bone marrow colored by cluster assignment (as in Figure 1B) (A), or by condition (control, light gray; leukemia, dark gray) (B).

(C and D) Compositional changes in bone marrow stroma. Binomial fit mean as percent of cells (y axis) assigned to specific cluster (C) or to Lepr-MSC and OLCs subclusters (D) among control or leukemic samples (x axis). Error bars: 95% confidence interval of the binomial fit mean.

(E) Changes in *Grem1* expression in Lepr-MSCs and OLCs. Average of samples (TP10K, y axis) in Lepr-MSC and OLC subclusters (x axis). Error bars, SEM.

(F–H) Changes in niche remodeling (F), hypoxia (G) and hematopoietic regulator genes (H) in Lepr-MSCs, OLC-1 s, and sBMECs in leukemia. Average expression (TP10K, y axis) of niche genes in Lepr-MSCs (top) and OLC-1s (bottom). Error bars, SEM.

(I and J) Changes in *Cxcl12*, *Kitl*, and *Angpt1* expression in BMECs, pericytes (I), or fibroblasts (J). Average expression (TP10K, y axis) of the denoted genes in specific cell clusters. Error bars, SEM.

(K) A census of the bone marrow stroma in homeostasis and leukemia. Horizontal boxes: broad cell types, with subsets noted. Circles: expression levels of key niche factors, *Kitl* and *Cxcl12*. Dark arrows: changes in subset proportion in leukemia. Colored arrows: changes in relative expression in leukemia.

See also Figure S7 and Tables S1 and S4.

in a cell-autonomous manner to cancer cells, but may extend to the broader cell context of a cancerous tissue. These findings are consistent with a model where emerging cancer cells influence the stromal cells in the tissue they inhabit. They can alter differentiation patterns of those stromal cells, changing the complexity of cell types that are thought to play critical roles in governing tissue homeostasis. Furthermore, the malignant cells in our study reduced the expression of regulatory signaling molecules known to be essential for normal hematopoietic function. In so doing, the malignant cells create a microenvironment no longer as conducive to normal hematopoietic cell production and, thereby, impairing the parenchymal cells with which they compete. These data provide experimental support for a paradigm in which the establishment of a malignant clone within a tissue shapes the features of the stromal landscape of that tissue. The result compromises stromal cell support of normal parenchymal cells, fundamentally altering the competitive landscape of the tissue to disadvantage normal cells. In this way, cancer cells act not as fully independent and destructive rogues, but rather as self-serving architects of their neighborhood pushing out normal occupants by creating a less supportive environment.

Our stroma cell census will now allow a clearer and more consistent definition of the ways in which specific stromal cells contribute to homeostasis and aberrant hematopoiesis and provide a foundation for developing stromal-targeted therapies in hematologic disease. It also offers experimental evidence for tumor evolution in which cross-communication between parenchymal and stromal elements may influence the emergence of cancer.

STAR★METHODS

Detailed methods are provided in the online version of this paper and include the following:

SUPPLEMENTAL INFORMATION

Supplemental Information can be found online at https://doi.org/10.1016/j.cell.2019.04.040.

ACKNOWLEDGMENTS

We thank Professor Henry Kronenberg for helpful comments, Leslie Gaffney and Anna Hupalowska for helping with figures, and Carl de Boer, Christopher Smillie, Adam Haber, Joshua Gould, and Bo Li for additional help. N.B. was funded by the Swedish Research Council and The Childhood Cancer Foundation in Sweden. M.S.K. was supported by Charles A. King Trust Postdoctoral Research Fellowship Program and the Simeon J. Fortin Charitable Foundation. Work was supported by the Klarman Cell Observatory and HHMI (to A.R.), NIH (DK107784), and the Gerald and Darlene Jordan Professorship (to D.T.S.).

AUTHOR CONTRIBUTIONS

Conceptualization, N.B., D.P., M.S.K., A.R. and D.T.S; Investigation, N.B., M.S.K., N.S., K.G., A.P., F.M., D.D., K.D.K., M.H., D.D., O.R.-R. and D.L; Validation, N.B. and K.D.K.; Computational Investigation and Analysis, D.P. with help and code contributions from M.T., M.H., A.S., O.A., and E.D.V.; Writing – Original Draft, N.B., D.P., M.K., A.R. and D.T.S.; Writing – Review & Editing, N.B., D.P., M.K., Y.K., N.S., K.D.K., A.R., and D.T.S; Funding Acquisition, Resources, & Supervision, A.R. and D.T.S.

DECLARATION OF INTERESTS

D.T.S. is a director and shareholder of Magenta Therapeutics, Agios Pharmaceuticals, Editas Medicines, Clear Creek Bio, Red Oak Medicines, and LifeVaultBio, a shareholder of Fate Therapeutics, a consultant for Magenta Therapeutics, Clear Creek Bio, Red Oak Medicines, and VCanBio, and a SAB member of FOG Pharma. A.R. is a founder and equity holder of Celsius Therapeutics and a member of the SAB for ThermoFisher Scientific and Syros Pharmaceuticals. M.S.K. is employed by Celsius Therapeutics. The authors have filed for a patent (62/808,177).

Received: December 11, 2018
Revised: March 5, 2019
Accepted: April 23, 2019
Published: May 23, 2019

REFERENCES

Abdallah, B.M., Al-Shammary, A., Skagen, P., Abu Dawud, R., Adjaye, J., Aldahmash, A., and Kassem, M. (2015). CD34 defines an osteoprogenitor cell population in mouse bone marrow stromal cells. Stem Cell Res. (Amst.) *15*, 449–458.

Acar, M., Kocherlakota, K.S., Murphy, M.M., Peyer, J.G., Oguro, H., Inra, C.N., Jaiyeola, C., Zhao, Z., Luby-Phelps, K., and Morrison, S.J. (2015). Deep imaging of bone marrow shows non-dividing stem cells are mainly perisinusoidal. Nature *526*, 126–130.

Ahirwar, D.K., Nasser, M.W., Ouseph, M.M., Elbaz, M., Cuitiño, M.C., Kladney, R.D., Varikuti, S., Kaul, K., Satoskar, A.R., Ramaswamy, B., et al. (2018). Fibroblast-derived CXCL12 promotes breast cancer metastasis by facilitating tumor cell intravasation. Oncogene *37*, 4428–4442.

Angerer, P., Haghverdi, L., Büttner, M., Theis, F.J., Marr, C., and Buettner, F. (2016). destiny: diffusion maps for large-scale single-cell data in R. Bioinformatics *32*, 1241–1243.

Arai, F., Hirao, A., Ohmura, M., Sato, H., Matsuoka, S., Takubo, K., Ito, K., Koh, G.Y., and Suda, T. (2004). Tie2/angiopoietin-1 signaling regulates hematopoietic stem cell quiescence in the bone marrow niche. Cell *118*, 149–161.

Armulik, A., Genové, G., and Betsholtz, C. (2011). Pericytes: developmental, physiological, and pathological perspectives, problems, and promises. Dev. Cell *21*, 193–215.

Arnold, M.A., Kim, Y., Czubryt, M.P., Phan, D., McAnally, J., Qi, X., Shelton, J.M., Richardson, J.A., Bassel-Duby, R., and Olson, E.N. (2007). MEF2C transcription factor controls chondrocyte hypertrophy and bone development. Dev. Cell *12*, 377–389.

Arranz, L., Sánchez-Aguilera, A., Martín-Pérez, D., Isern, J., Langa, X., Tzankov, A., Lundberg, P., Muntión, S., Tzeng, Y.S., Lai, D.M., et al. (2014). Neuropathy of haematopoietic stem cell niche is essential for myeloproliferative neoplasms. Nature *512*, 78–81.

Bastian, M., Heymann, S., and Jacomy, M. (2009). Gephi: an open source software for exploring and manipulating networks. International AAAI Conference on Web and Social Media, North America *8*, 361–362.

Bauche, I.B., El Mkadem, S.A., Pottier, A.M., Senou, M., Many, M.C., Rezsohazy, R., Penicaud, L., Maeda, N., Funahashi, T., and Brichard, S.M. (2007). Overexpression of adiponectin targeted to adipose tissue in transgenic mice: impaired adipocyte differentiation. Endocrinology *148*, 1539–1549.

Benjamini, Y., and Hochberg, Y. (1995). Controlling the false discovery rate: a practical and powerful approach to multiple testing. J. R. Stat. Soc. Series B *57*, 289–300.

Bernad, A., Kopf, M., Kulbacki, R., Weich, N., Koehler, G., and Gutierrez-Ramos, J.C. (1994). Interleukin-6 is required in vivo for the regulation of stem cells and committed progenitors of the hematopoietic system. Immunity *1*, 725–731.

Beygelzimer, A., Kakadet, S., Langford, J., Arya, S., Mount, D., and Li, S. (2015). Package 'FNN' (University of Maryland).

Blondel, V.D., Guillaume, J.-L., Lambiotte, R., and Lefebvre, E. (2008). Fast unfolding of communities in large networks. arXiv. https://doi.org/10.1088/1742-5468/2008/10/P10008.

Boyd, A.L., Reid, J.C., Salci, K.R., Aslostovar, L., Benoit, Y.D., Shapovalova, Z., Nakanishi, M., Porras, D.P., Almakadi, M., Campbell, C.J.V., et al. (2017). Acute myeloid leukaemia disrupts endogenous myelo-erythropoiesis by compromising the adipocyte bone marrow niche. Nat. Cell Biol. *19*, 1336–1347.

Butler, J.M., Nolan, D.J., Vertes, E.L., Varnum-Finney, B., Kobayashi, H., Hooper, A.T., Seandel, M., Shido, K., White, I.A., Kobayashi, M., et al. (2010). Endothelial cells are essential for the self-renewal and repopulation of Notch-dependent hematopoietic stem cells. Cell Stem Cell *6*, 251–264.

Calvi, L.M., Adams, G.B., Weibrecht, K.W., Weber, J.M., Olson, D.P., Knight, M.C., Martin, R.P., Schipani, E., Divieti, P., Bringhurst, F.R., et al. (2003). Osteoblastic cells regulate the haematopoietic stem cell niche. Nature *425*, 841–846.

Chan, D., Cole, W.G., Chow, C.W., Mundlos, S., and Bateman, J.F. (1995). A COL2A1 mutation in achondrogenesis type II results in the replacement of type II collagen by type I and III collagens in cartilage. J. Biol. Chem. *270*, 1747–1753.

Chan, C.K., Seo, E.Y., Chen, J.Y., Lo, D., McArdle, A., Sinha, R., Tevlin, R., Seita, J., Vincent-Tompkins, J., Wearda, T., et al. (2015). Identification and specification of the mouse skeletal stem cell. Cell *160*, 285–298.

Chen, Y.B., Ren, S.M., Li, S.D., and Du, Z. (2017). Prognostic significance of osteopontin in acute myeloid leukemia: A meta-analysis. Mol. Clin. Oncol. *7*, 275–280.

Corada, M., Liao, F., Lindgren, M., Lampugnani, M.G., Breviario, F., Frank, R., Muller, W.A., Hicklin, D.J., Bohlen, P., and Dejana, E. (2001). Monoclonal antibodies directed to different regions of vascular endothelial cadherin extracellular domain affect adhesion and clustering of the protein and modulate endothelial permeability. Blood *97*, 1679–1684.

Corral, J., Lavenir, I., Impey, H., Warren, A.J., Forster, A., Larson, T.A., Bell, S., McKenzie, A.N., King, G., and Rabbitts, T.H. (1996). An Mll-AF9 fusion gene made by homologous recombination causes acute leukemia in chimeric mice: a method to create fusion oncogenes. Cell *85*, 853–861.

Costa, A., Kieffer, Y., Scholer-Dahirel, A., Pelon, F., Bourachot, B., Cardon, M., Sirven, P., Magagna, I., Fuhrmann, L., Bernard, C., et al. (2018). Fibroblast Heterogeneity and Immunosuppressive Environment in Human Breast Cancer. Cancer Cell *33*, 463–479.

Coutu, D.L., Kokkaliaris, K.D., Kunz, L., and Schroeder, T. (2017). Three-dimensional map of nonhematopoietic bone and bone-marrow cells and molecules. Nat. Biotechnol. *35*, 1202–1210.

Coutu, D.L., Kokkaliaris, K.D., Kunz, L., and Schroeder, T. (2018). Multicolor quantitative confocal imaging cytometry. Nat. Methods *15*, 39–46.

Delmas, P.D., Demiaux, B., Malaval, L., Chapuy, M.C., and Meunier, P.J. (1986). [Osteocalcin (or bone gla-protein), a new biological marker for studying bone pathology]. Presse Med. *15*, 643–646.

Ding, L., and Morrison, S.J. (2013). Haematopoietic stem cells and early lymphoid progenitors occupy distinct bone marrow niches. Nature *495*, 231–235.

Ding, L., Saunders, T.L., Enikolopov, G., and Morrison, S.J. (2012). Endothelial and perivascular cells maintain haematopoietic stem cells. Nature *481*, 457–462.

Doan, P.L., Russell, J.L., Himburg, H.A., Helms, K., Harris, J.R., Lucas, J., Holshausen, K.C., Meadows, S.K., Daher, P., Jeffords, L.B., et al. (2013). Tie2(+) bone marrow endothelial cells regulate hematopoietic stem cell regeneration following radiation injury. Stem Cells *31*, 327–337.

Doege, K.J., Sasaki, M., Kimura, T., and Yamada, Y. (1991). Complete coding sequence and deduced primary structure of the human cartilage large aggregating proteoglycan, aggrecan. Human-specific repeats, and additional alternatively spliced forms. J. Biol. Chem. *266*, 894–902.

Dominici, M., Le Blanc, K., Mueller, I., Slaper-Cortenbach, I., Marini, F., Krause, D., Deans, R., Keating, A., Prockop, Dj., and Horwitz, E. (2006). Minimal criteria for defining multipotent mesenchymal stromal cells. The International Society for Cellular Therapy position statement. Cytotherapy *8*, 315–317.

Dong, L., Yu, W.M., Zheng, H., Loh, M.L., Bunting, S.T., Pauly, M., Huang, G., Zhou, M., Broxmeyer, H.E., Scadden, D.T., and Qu, C.K. (2016). Leukaemogenic effects of Ptpn11 activating mutations in the stem cell microenvironment. Nature *539*, 304–308.

Duarte, D., Hawkins, E.D., Akinduro, O., Ang, H., De Filippo, K., Kong, I.Y., Haltalli, M., Ruivo, N., Straszkowski, L., Vervoort, S.J., et al. (2018). Inhibition of Endosteal Vascular Niche Remodeling Rescues Hematopoietic Stem Cell Loss in AML. Cell Stem Cell *22*, 64–77.

Foster, J.W., Dominguez-Steglich, M.A., Guioli, S., Kwok, C., Weller, P.A., Stevanović, M., Weissenbach, J., Mansour, S., Young, I.D., Goodfellow, P.N., et al. (1994). Campomelic dysplasia and autosomal sex reversal caused by mutations in an SRY-related gene. Nature *372*, 525–530.

Frisch, B.J., Ashton, J.M., Xing, L., Becker, M.W., Jordan, C.T., and Calvi, L.M. (2012). Functional inhibition of osteoblastic cells in an in vivo mouse model of myeloid leukemia. Blood *119*, 540–550.

Fuady, J.H., Bordoli, M.R., Abreu-Rodriguez, I., Kristiansen, G., Hoogewijs, D., Stiehl, D.P., and Wenger, R.H. (2014). Hypoxia-inducible factor-mediated induction of WISP-2 contributes to attenuated progression of breast cancer. Hypoxia *2*, 23–33.

Geyh, S., Rodríguez-Paredes, M., Jäger, P., Khandanpour, C., Cadeddu, R.P., Gutekunst, J., Wilk, C.M., Fenk, R., Zilkens, C., Hermsen, D., et al. (2016). Functional inhibition of mesenchymal stromal cells in acute myeloid leukemia. Leukemia *30*, 683–691.

Gomei, Y., Nakamura, Y., Yoshihara, H., Hosokawa, K., Iwasaki, H., Suda, T., and Arai, F. (2010). Functional differences between two Tie2 ligands, angiopoietin-1 and -2, in regulation of adult bone marrow hematopoietic stem cells. Exp. Hematol. *38*, 82–89.

Greenbaum, A., Hsu, Y.M., Day, R.B., Schuettpelz, L.G., Christopher, M.J., Borgerding, J.N., Nagasawa, T., and Link, D.C. (2013). CXCL12 in early

mesenchymal progenitors is required for haematopoietic stem-cell maintenance. Nature *495*, 227–230.

Grünberg, J.R., Hammarstedt, A., Hedjazifar, S., and Smith, U. (2014). The Novel Secreted Adipokine WNT1-inducible Signaling Pathway Protein 2 (WISP2) Is a Mesenchymal Cell Activator of Canonical WNT. J. Biol. Chem. *289*, 6899–6907.

Hammarstedt, A., Hedjazifar, S., Jenndahl, L., Gogg, S., Grünberg, J., Gustafson, B., Klimcakova, E., Stich, V., Langin, D., Laakso, M., and Smith, U. (2013). WISP2 regulates preadipocyte commitment and PPARγ activation by BMP4. Proc. Natl. Acad. Sci. USA *110*, 2563–2568.

Hanoun, M., Zhang, D., Mizoguchi, T., Pinho, S., Pierce, H., Kunisaki, Y., Lacombe, J., Armstrong, S.A., Dührsen, U., and Frenette, P.S. (2014). Acute myelogenous leukemia-induced sympathetic neuropathy promotes malignancy in an altered hematopoietic stem cell niche. Cell Stem Cell *15*, 365–375.

Hawkins, E.D., Duarte, D., Akinduro, O., Khorshed, R.A., Passaro, D., Nowicka, M., Straszkowski, L., Scott, M.K., Rothery, S., Ruivo, N., et al. (2016). T-cell acute leukaemia exhibits dynamic interactions with bone marrow microenvironments. Nature *538*, 518–522.

Hooper, A.T., Butler, J.M., Nolan, D.J., Kranz, A., Iida, K., Kobayashi, M., Kopp, H.G., Shido, K., Petit, I., Yanger, K., et al. (2009). Engraftment and reconstitution of hematopoiesis is dependent on VEGFR2-mediated regeneration of sinusoidal endothelial cells. Cell Stem Cell *4*, 263–274.

Huang, W., Yang, S., Shao, J., and Li, Y.P. (2007). Signaling and transcriptional regulation in osteoblast commitment and differentiation. Front. Biosci. *12*, 3068–3092.

Inada, M., Yasui, T., Nomura, S., Miyake, S., Deguchi, K., Himeno, M., Sato, M., Yamagiwa, H., Kimura, T., Yasui, N., et al. (1999). Maturational disturbance of chondrocytes in Cbfa1-deficient mice. Dev. Dyn. *214*, 279–290.

Itkin, T., Gur-Cohen, S., Spencer, J.A., Schajnovitz, A., Ramasamy, S.K., Kusumbe, A.P., Ledergor, G., Jung, Y., Milo, I., Poulos, M.G., et al. (2016). Distinct bone marrow blood vessels differentially regulate haematopoiesis. Nature *532*, 323–328.

Jacomy, M., Venturini, T., Heymann, S., and Bastian, M. (2014). ForceAtlas2, a continuous graph layout algorithm for handy network visualization designed for the Gephi software. PLoS ONE *9*, e98679.

Kalluri, R. (2016). The biology and function of fibroblasts in cancer. Nat. Rev. Cancer *16*, 582–598.

Kanatani, M., Sugimoto, T., Nishiyama, K., and Chihara, K. (2000). Stimulatory effect of insulin-like growth factor binding protein-5 on mouse osteoclast formation and osteoclastic bone-resorbing activity. J. Bone Miner. Res. *15*, 902–910.

Kfoury, Y., and Scadden, D.T. (2015). Mesenchymal cell contributions to the stem cell niche. Cell Stem Cell *16*, 239–253.

Kim, Y., Lin, Q., Glazer, P.M., and Yun, Z. (2009). Hypoxic tumor microenvironment and cancer cell differentiation. Curr. Mol. Med. *9*, 425–434.

Kobayashi, H., Butler, J.M., O'Donnell, R., Kobayashi, M., Ding, B.S., Bonner, B., Chiu, V.K., Nolan, D.J., Shido, K., Benjamin, L., and Rafii, S. (2010). Angiocrine factors from Akt-activated endothelial cells balance self-renewal and differentiation of haematopoietic stem cells. Nat. Cell Biol. *12*, 1046–1056.

Kode, A., Manavalan, J.S., Mosialou, I., Bhagat, G., Rathinam, C.V., Luo, N., Khiabanian, H., Lee, A., Murty, V.V., Friedman, R., et al. (2014). Leukaemogenesis induced by an activating β-catenin mutation in osteoblasts. Nature *506*, 240–244.

Kowalczyk, M.S., Tirosh, I., Heckl, D., Rao, T.N., Dixit, A., Haas, B.J., Schneider, R.K., Wagers, A.J., Ebert, B.L., and Regev, A. (2015). Single-cell RNA-seq reveals changes in cell cycle and differentiation programs upon aging of hematopoietic stem cells. Genome Res. *25*, 1860–1872.

Krevvata, M., Silva, B.C., Manavalan, J.S., Galan-Diez, M., Kode, A., Matthews, B.G., Park, D., Zhang, C.A., Galili, N., Nickolas, T.L., et al. (2014). Inhibition of leukemia cell engraftment and disease progression in mice by osteoblasts. Blood *124*, 2834–2846.

Kumar, B., Garcia, M., Weng, L., Jung, X., Murakami, J.L., Hu, X., McDonald, T., Lin, A., Kumar, A.R., DiGiusto, D.L., et al. (2018). Acute myeloid leukemia transforms the bone marrow niche into a leukemia-permissive microenvironment through exosome secretion. Leukemia *32*, 575–587.

Kunisaki, Y., Bruns, I., Scheiermann, C., Ahmed, J., Pinho, S., Zhang, D., Mizoguchi, T., Wei, Q., Lucas, D., Ito, K., et al. (2013). Arteriolar niches maintain haematopoietic stem cell quiescence. Nature *502*, 637–643.

Kusumbe, A.P., Ramasamy, S.K., Itkin, T., Mäe, M.A., Langen, U.H., Betsholtz, C., Lapidot, T., and Adams, R.H. (2016). Age-dependent modulation of vascular niches for haematopoietic stem cells. Nature *532*, 380–384.

Lara-Castro, C., Fu, Y., Chung, B.H., and Garvey, W.T. (2007). Adiponectin and the metabolic syndrome: mechanisms mediating risk for metabolic and cardiovascular disease. Curr. Opin. Lipidol. *18*, 263–270.

Lee, N.K., Sowa, H., Hinoi, E., Ferron, M., Ahn, J.D., Confavreux, C., Dacquin, R., Mee, P.J., McKee, M.D., Jung, D.Y., et al. (2007). Endocrine regulation of energy metabolism by the skeleton. Cell *130*, 456–469.

Liaw, A., and Wiener, M. (2002). Classification and regression by randomforest. R News *2*, 18–22.

Lo Celso, C., Fleming, H.E., Wu, J.W., Zhao, C.X., Miake-Lye, S., Fujisaki, J., Côté, D., Rowe, D.W., Lin, C.P., and Scadden, D.T. (2009). Live-animal tracking of individual haematopoietic stem/progenitor cells in their niche. Nature *457*, 92–96.

Luo, G., Ducy, P., McKee, M.D., Pinero, G.J., Loyer, E., Behringer, R.R., and Karsenty, G. (1997). Spontaneous calcification of arteries and cartilage in mice lacking matrix GLA protein. Nature *386*, 78–81.

Mabuchi, Y., Morikawa, S., Harada, S., Niibe, K., Suzuki, S., Renault-Mihara, F., Houlihan, D.D., Akazawa, C., Okano, H., and Matsuzaki, Y. (2013). LNGFR(+)THY-1(+)VCAM-1(hi+) cells reveal functionally distinct subpopulations in mesenchymal stem cells. Stem Cell Reports *1*, 152–165.

Méndez-Ferrer, S., Michurina, T.V., Ferraro, F., Mazloom, A.R., Macarthur, B.D., Lira, S.A., Scadden, D.T., Ma'ayan, A., Enikolopov, G.N., and Frenette, P.S. (2010). Mesenchymal and haematopoietic stem cells form a unique bone marrow niche. Nature *466*, 829–834.

Mercier, F.E., Sykes, D.B., and Scadden, D.T. (2016). Single Targeted Exon Mutation Creates a True Congenic Mouse for Competitive Hematopoietic Stem Cell Transplantation: The C57BL/6-CD45.1(STEM) Mouse. Stem Cell Reports *6*, 985–992.

Morrison, S.J., and Scadden, D.T. (2014). The bone marrow niche for haematopoietic stem cells. Nature *505*, 327–334.

Mossadegh-Keller, N., Sarrazin, S., Kandalla, P.K., Espinosa, L., Stanley, E.R., Nutt, S.L., Moore, J., and Sieweke, M.H. (2013). M-CSF instructs myeloid lineage fate in single haematopoietic stem cells. Nature *497*, 239–243.

Muegge, K., Vila, M.P., and Durum, S.K. (1993). Interleukin-7: a cofactor for V(D)J rearrangement of the T cell receptor beta gene. Science *261*, 93–95.

Nakashima, K., Zhou, X., Kunkel, G., Zhang, Z., Deng, J.M., Behringer, R.R., and de Crombrugghe, B. (2002). The novel zinc finger-containing transcription factor osterix is required for osteoblast differentiation and bone formation. Cell *108*, 17–29.

Namen, A.E., Lupton, S., Hjerrild, K., Wignall, J., Mochizuki, D.Y., Schmierer, A., Mosley, B., March, C.J., Urdal, D., and Gillis, S. (1988). Stimulation of B-cell progenitors by cloned murine interleukin-7. Nature *333*, 571–573.

Nilsson, S.K., Johnston, H.M., Whitty, G.A., Williams, B., Webb, R.J., Denhardt, D.T., Bertoncello, I., Bendall, L.J., Simmons, P.J., and Haylock, D.N. (2005). Osteopontin, a key component of the hematopoietic stem cell niche and regulator of primitive hematopoietic progenitor cells. Blood *106*, 1232–1239.

Nishimura, R., Wakabayashi, M., Hata, K., Matsubara, T., Honma, S., Wakisaka, S., Kiyonari, H., Shioi, G., Yamaguchi, A., Tsumaki, N., et al. (2012). Osterix regulates calcification and degradation of chondrogenic matrices through matrix metalloproteinase 13 (MMP13) expression in association with transcription factor Runx2 during endochondral ossification. J. Biol. Chem. *287*, 33179–33190.

Papayannopoulou, T., Craddock, C., Nakamoto, B., Priestley, G.V., and Wolf, N.S. (1995). The VLA4/VCAM-1 adhesion pathway defines contrasting

mechanisms of lodgement of transplanted murine hemopoietic progenitors between bone marrow and spleen. Proc. Natl. Acad. Sci. USA *92*, 9647–9651.

Park, D., Spencer, J.A., Koh, B.I., Kobayashi, T., Fujisaki, J., Clemens, T.L., Lin, C.P., Kronenberg, H.M., and Scadden, D.T. (2012). Endogenous bone marrow MSCs are dynamic, fate-restricted participants in bone maintenance and regeneration. Cell Stem Cell *10*, 259–272.

Passaro, D., Di Tullio, A., Abarrategi, A., Rouault-Pierre, K., Foster, K., Ariza-McNaughton, L., Montaner, B., Chakravarty, P., Bhaw, L., Diana, G., et al. (2017). Increased vascular permeability in the bone marrow microenvironment contributes to disease progression and drug response in acute myeloid leukemia. Cancer Cell *32*, 324–341.

Pittenger, M.F., Mackay, A.M., Beck, S.C., Jaiswal, R.K., Douglas, R., Mosca, J.D., Moorman, M.A., Simonetti, D.W., Craig, S., and Marshak, D.R. (1999). Multilineage potential of adult human mesenchymal stem cells. Science *284*, 143–147.

Raaijmakers, M.H., Mukherjee, S., Guo, S., Zhang, S., Kobayashi, T., Schoonmaker, J.A., Ebert, B.L., Al-Shahrour, F., Hasserjian, R.P., Scadden, E.O., et al. (2010). Bone progenitor dysfunction induces myelodysplasia and secondary leukaemia. Nature *464*, 852–857.

Rafii, S., Butler, J.M., and Ding, B.S. (2016). Angiocrine functions of organ-specific endothelial cells. Nature *529*, 316–325.

Rauner, M., Franke, K., Murray, M., Singh, R.P., Hiram-Bab, S., Platzbecker, U., Gassmann, M., Socolovsky, M., Neumann, D., Gabet, Y., et al. (2016). Increased EPO Levels Are Associated With Bone Loss in Mice Lacking PHD2 in EPO-Producing Cells. J. Bone Miner. Res. *31*, 1877–1887.

Satija, R., Farrell, J.A., Gennert, D., Schier, A.F., and Regev, A. (2015). Spatial reconstruction of single-cell gene expression data. Nat. Biotechnol. *33*, 495–502.

Scadden, D.T. (2014). Nice neighborhood: emerging concepts of the stem cell niche. Cell *157*, 41–50.

Schepers, K., Pietras, E.M., Reynaud, D., Flach, J., Binnewies, M., Garg, T., Wagers, A.J., Hsiao, E.C., and Passegué, E. (2013). Myeloproliferative neoplasia remodels the endosteal bone marrow niche into a self-reinforcing leukemic niche. Cell Stem Cell *13*, 285–299.

Schiebinger, G., Shu, J., Tabaka, M., Cleary, B., Subramanian, V., Solomon, A., Liu, S., Lin, S., Berube, P., and Lee, L. (2017). Reconstruction of developmental landscapes by optimal-transport analysis of single-cell gene expression sheds light on cellular reprogramming. bioRxiv. https://doi.org/10.1101/191056.

Schmidt, T., Kharabi Masouleh, B., Loges, S., Cauwenberghs, S., Fraisl, P., Maes, C., Jonckx, B., De Keersmaecker, K., Kleppe, M., Tjwa, M., et al. (2011). Loss or inhibition of stromal-derived PlGF prolongs survival of mice with imatinib-resistant Bcr-Abl1(+) leukemia. Cancer Cell *19*, 740–753.

Schofield, R. (1978). The relationship between the spleen colony-forming cell and the haemopoietic stem cells. Blood Cells *4*, 7–25.

Silha, J.V., Mishra, S., Rosen, C.J., Beamer, W.G., Turner, R.T., Powell, D.R., and Murphy, L.J. (2003). Perturbations in bone formation and resorption in insulin-like growth factor binding protein-3 transgenic mice. J. Bone Miner. Res. *18*, 1834–1841.

Soundararajan, M., and Kannan, S. (2018). Fibroblasts and mesenchymal stem cells: Two sides of the same coin? J. Cell. Physiol. *233*, 9099–9109.

Stier, S., Ko, Y., Forkert, R., Lutz, C., Neuhaus, T., Grünewald, E., Cheng, T., Dombkowski, D., Calvi, L.M., Rittling, S.R., and Scadden, D.T. (2005). Osteopontin is a hematopoietic stem cell niche component that negatively regulates stem cell pool size. J. Exp. Med. *201*, 1781–1791.

Strutz, F., Okada, H., Lo, C.W., Danoff, T., Carone, R.L., Tomaszewski, J.E., and Neilson, E.G. (1995). Identification and characterization of a fibroblast marker: FSP1. J. Cell Biol. *130*, 393–405.

Subramanian, A., Tamayo, P., Mootha, V.K., Mukherjee, S., Ebert, B.L., Gillette, M.A., Paulovich, A., Pomeroy, S.L., Golub, T.R., Lander, E.S., and Mesirov, J.P. (2005). Gene set enrichment analysis: a knowledge-based approach for interpreting genome-wide expression profiles. Proc. Natl. Acad. Sci. USA *102*, 15545–15550.

Sugimoto, Y., Takimoto, A., Akiyama, H., Kist, R., Scherer, G., Nakamura, T., Hiraki, Y., and Shukunami, C. (2013). Scx+/Sox9+ progenitors contribute to the establishment of the junction between cartilage and tendon/ligament. Development *140*, 2280–2288.

Sugiyama, T., Kohara, H., Noda, M., and Nagasawa, T. (2006). Maintenance of the hematopoietic stem cell pool by CXCL12-CXCR4 chemokine signaling in bone marrow stromal cell niches. Immunity *25*, 977–988.

Tikhonova, A.N., Dolgalev, I., Hu, H., Sivaraj, K.K., Hoxha, E., Cuesta-Domínguez, Á., Pinho, S., Akhmetzyanova, I., Gao, J., Witkowski, M., et al. (2019). The bone marrow microenvironment at single-cell resolution. Nature. Published online April 10, 2019. https://doi.org/10.1038/s41586-019-1104-8.

Tirosh, I., Izar, B., Prakadan, S.M., Wadsworth, M.H., 2nd, Treacy, D., Trombetta, J.J., Rotem, A., Rodman, C., Lian, C., Murphy, G., et al. (2016). Dissecting the multicellular ecosystem of metastatic melanoma by single-cell RNA-seq. Science *352*, 189–196.

Tontonoz, P., Hu, E., and Spiegelman, B.M. (1994). Stimulation of adipogenesis in fibroblasts by PPAR gamma 2, a lipid-activated transcription factor. Cell *79*, 1147–1156.

van den Brink, S.C., Sage, F., Vértesy, Á., Spanjaard, B., Peterson-Maduro, J., Baron, C.S., Robin, C., and van Oudenaarden, A. (2017). Single-cell sequencing reveals dissociation-induced gene expression in tissue subpopulations. Nat. Methods *14*, 935–936.

van der Maaten, L., and Hinton, G. (2008). Visualizing data using t-SNE. J. Mach. Learn. Res. *9*, 2579–2605.

Vortkamp, A., Lee, K., Lanske, B., Segre, G.V., Kronenberg, H.M., and Tabin, C.J. (1996). Regulation of rate of cartilage differentiation by Indian hedgehog and PTH-related protein. Science *273*, 613–622.

Wagner, T., Wirth, J., Meyer, J., Zabel, B., Held, M., Zimmer, J., Pasantes, J., Bricarelli, F.D., Keutel, J., Hustert, E., et al. (1994). Autosomal sex reversal and campomelic dysplasia are caused by mutations in and around the SRY-related gene SOX9. Cell *79*, 1111–1120.

Wolf, F.A., Hamey, F., Plass, M., Solana, J., Dahlin, J.S., Gottgens, B., Rajewsky, N., Simon, L., and Theis, F.J. (2017). Graph abstraction reconciles clustering with trajectory inference through a topology preserving map of single cells. bioRxiv. https://doi.org/10.1101/208819.

Wolf, F.A., Angerer, P., and Theis, F.J. (2018). SCANPY: large-scale single-cell gene expression data analysis. Genome Biol. *19*, 15.

Worthley, D.L., Churchill, M., Compton, J.T., Tailor, Y., Rao, M., Si, Y., Levin, D., Schwartz, M.G., Uygur, A., Hayakawa, Y., et al. (2015). Gremlin 1 identifies a skeletal stem cell with bone, cartilage, and reticular stromal potential. Cell *160*, 269–284.

Wozney, J.M., Rosen, V., Celeste, A.J., Mitsock, L.M., Whitters, M.J., Kriz, R.W., Hewick, R.M., and Wang, E.A. (1988). Novel regulators of bone formation: molecular clones and activities. Science *242*, 1528–1534.

Xu, C., Gao, X., Wei, Q., Nakahara, F., Zimmerman, S.E., Mar, J., and Frenette, P.S. (2018). Stem cell factor is selectively secreted by arterial endothelial cells in bone marrow. Nat. Commun. *9*, 2449.

Yang, L., Tsang, K.Y., Tang, H.C., Chan, D., and Cheah, K.S. (2014). Hypertrophic chondrocytes can become osteoblasts and osteocytes in endochondral bone formation. Proc. Natl. Acad. Sci. USA *111*, 12097–12102.

Yu, V.W., Saez, B., Cook, C., Lotinun, S., Pardo-Saganta, A., Wang, Y.H., Lymperi, S., Ferraro, F., Raaijmakers, M.H., Wu, J.Y., et al. (2015). Specific bone cells produce DLL4 to generate thymus-seeding progenitors from bone marrow. J. Exp. Med. *212*, 759–774.

Yu, V.W., Lymperi, S., Oki, T., Jones, A., Swiatek, P., Vasic, R., Ferraro, F., and Scadden, D.T. (2016). Distinctive Mesenchymal-Parenchymal Cell Pairings Govern B Cell Differentiation in the Bone Marrow. Stem Cell Reports *7*, 220–235.

Zambetti, N.A., Ping, Z., Chen, S., Kenswil, K.J.G., Mylona, M.A., Sanders, M.A., Hoogenboezem, R.M., Bindels, E.M.J., Adisty, M.N., Van Strien, P.M.H., et al. (2016). Mesenchymal Inflammation Drives Genotoxic Stress in Hematopoietic Stem Cells and Predicts Disease Evolution in Human Pre-leukemia. Cell Stem Cell *19*, 613–627.

Zhang, J., Niu, C., Ye, L., Huang, H., He, X., Tong, W.G., Ross, J., Haug, J., Johnson, T., Feng, J.Q., et al. (2003). Identification of the haematopoietic stem cell niche and control of the niche size. Nature *425*, 836–841.

Zhang, B., Ho, Y.W., Huang, Q., Maeda, T., Lin, A., Lee, S.U., Hair, A., Holyoake, T.L., Huettner, C., and Bhatia, R. (2012). Altered microenvironmental regulation of leukemic and normal stem cells in chronic myelogenous leukemia. Cancer Cell *21*, 577–592.

Zhou, B.O., Yue, R., Murphy, M.M., Peyer, J.G., and Morrison, S.J. (2014a). Leptin-receptor-expressing mesenchymal stromal cells represent the main source of bone formed by adult bone marrow. Cell Stem Cell *15*, 154–168.

Zhou, X., von der Mark, K., Henry, S., Norton, W., Adams, H., and de Crombrugghe, B. (2014b). Chondrocytes transdifferentiate into osteoblasts in endochondral bone during development, postnatal growth and fracture healing in mice. PLoS Genet. *10*, e1004820.

STAR★METHODS

KEY RESOURCES TABLE

REAGENT or RESOURCE	SOURCE	IDENTIFIER
Antibodies		
CD45	eBioscience	Cat#12-0451-82; RRID:AB_465668
CD45.1	Biolegend	Cat#110706; RRID:AB_313495
CD45.2	Biolegend	Cat#109824; RRID: AB_830789
B220	eBioscience/Biolegend	Cat#48-0452-82 & 103208; RRID: AB_1548761 & AB_312993
CD19	Biolegend	Cat#115508; RRID: AB_313643
Mac1 (CD11b)	Biolegend	Cat#101222 & 101208; RRID: AB_493705 & AB_312791
Gr1	Biolegend	Cat#108431 & 108408; RRID: AB_10896783 & AB_313373
CD3e	eBioscience/Biolegend	Cat#17-0031-83 & 100206; RRID: AB_469316 & AB_312663
Ter-119	eBioscience/Biolegend	Cat#17-5921-82/113812; RRID: AB_469473 & AB_2203382
CD31 (Pecam1)	BD Bioscience/R&D Systems	Cat#565097 & AF3628; RRID: AB_2739066 & AB_2161028
CD105 (Pdgfra)	Biolegend	Cat#120410; RRID: AB_1027700
CD90 (Thy1)	Biolegend	Cat#105331; RRID: AB_2562900
Sca1 (Ly6a)	Biolegend	Cat#108127; RRID: AB_10898327
Vcam1	Biolegend	Cat#105710; RRID: AB_493427
CD71	Biolegend	Cat#113812; RRID: AB_2203382
CD144 (VE-Cadherin/Cdh5)	Biolegend	Cat#138006; RRID: AB_10569114
CD130 (Il6st)	Biolegend	Cat# 362006; RRID: AB_2563404
CD34	eBioscience	Cat#11-0341-82; RRID: AB_465021
Collagen type I	Cedarlene,	Cat# CL50151AP; RRID: AB_10061240
von Willenbrand factor	ThermoScientific	Cat#RB-281-AO
Endomucin	eBiosciences	Cat#14-5851-82; RRID: AB_891527
Secondary antibodies (CF488, CF555, CF633 and CF680)	Biotium	N/A
Critical Commercial Assays		
Chromium Single Cell 3′v2 Reagent Kit	10X Genomics	N/A
Deposited Data		
Sequencing Reads, feature-barcode matrices	GEO	GSE128423
Experimental Models: Organisms/Strains		
CD45.1 STEM (males, 8-10 weeks old)	Mercier et al., 2016	https://doi.org/10.1016/j.stemcr.2016.04.010
Kmt2atm2(MLLT3)Thr/KsyJ (males, 8-10 weeks old)	Jackson Laboratory	Cat#9079
C57BL/6J (males, 8-10 weeks old)	Jackson Laboratory	Cat#664
Software and Algorithms		
cellranger-2.0.1	N/A	https://support.10xgenomics.com/single-cell-gene-expression/software/downloads/latest
R-3.4.1	N/A	https://cran.r-project.org/mirrors.html
Seurat 2.3.4	N/A	https://cran.r-project.org/web/packages/Seurat/index.html
Other		
Media 199	Thermofisher Scientific	Cat#12350039
STEMxyme1	Worthington	Cat#LS004106
Dispase II	Thermofisher Scientific	Cat#17105041
ACK-lysis buffer	Thermofisher Scientific	Cat#A1049201

(*Continued on next page*)

Continued

REAGENT or RESOURCE	SOURCE	IDENTIFIER
Calcein AM	Thermofisher Scientific	Cat#C3099
7-AAD	Thermofisher Scientific	Cat#00-6993-50
Ultrapure BSA	Thermofisher Scientific	Cat#AM2616
Confocal microscope	Leica	Leica TCS SP8

CONTACT FOR REAGENT AND RESOURCE SHARING

Further information and requests for resources and reagents should be directed to and will be fulfilled by the lead contact David Scadden (david_scadden@harvard.edu).

EXPERIMENTAL MODEL AND SUBJECT DETAILS

Mice

The MLL-AF9 knock-in mice (Corral et al., 1996) and CD45.1 (STEM) mice (Mercier et al., 2016) were described previously. Littermates were used as controls for all experiments involving MLL-AF9 knockin and CD45.1 (STEM) mice. Male C57BL/6 mice (CD45.2, Jackson Laboratory) at age 6-8 weeks were employed as transplant recipients and for steady-state scRNA-seq experiments. All animal experiments were performed in accordance with national and institutional guidelines. Mice were housed in the Massachusetts General Hospital (MGH) Animal Research Facility on a 12 hour light/dark cycle with stable temperature (22°C) and humidity (60%). All procedures were approved by MGH Internal Animal Care and Use Committee.

Generation of leukemic mice

To generate leukemic mice, we first crossed the MLL-AF9 knock-in mice (Corral et al., 1996) with the CD45.1 (STEM) mice (Mercier et al., 2016) to generate donor chimeric CD45.1.2 mice. Mice positive for the MLL-AF9 fusion transgene were used as donors (male, 4 weeks of age), and littermates (male, 4 weeks of age) negative for the MLL-AF9 fusion transgene were used as controls. Mice were sacrificed via CO_2 asphyxia; tibiae and femurs were harvested and excess soft tissue was eliminated. Bones were crushed and washed in PBS and passed through a 70 μm filter into a collection tube and$1x10^6$ whole bone-marrow cells were transplanted by retro-orbital injection into 6-8 weeks old male CD45.2 C57BL/6 recipient mice. One day prior to transplantation, mice were subjected to whole-body irradiation (2 × 6Gy) with a 6-hour interval from a ^{137}Cs source. Monthly retro-orbital bleeding was performed on isoflurane anesthetized mice and blood was withdrawn using heparinized capillaries and collected into EDTA containing tubes to prevent coagulation. Complete blood counts were done using the Element Ht5 Auto Hematology analyzer. Subsequently, RBCs were lysed as described previously and cells were stained in PBS, 2% FBS using the following antibodies: CD45.2-APCCy7 (Biolegend, Ref#109824, clone 102), CD45.1-FITC (Biolegend, Ref# 110706, clone A20), CD11b-Alexa Fluor 700 (Biolegend, Ref# 101222, clone M1/70), GR1-Brilliant violet 570 (Biolegend, Ref#108431, clone RB6-8C5), B220-eFluor450 (eBioscience, Ref#48-0452-82, clone RA3-6B2), and CD3e-APC (eBioscience, Ref#17-0031-83, clone 145-2c11), in addition to 7-Aminoactinomycin D (7AAD; ThermoFisher Scientific, Ref#A1310) for viability to monitor donor chimerism within the different lineages and the appearance of leukemic blasts characterized by a distinct scatter and lower GR1 and CD11b expression within the myeloid compartment. Leukemic mice were determined by the combination of disease symptoms, white blood cell counts and appearance of leukemic blasts.

METHOD DETAILS

Isolation of bone marrow stromal cells

To obtain bone and bone marrow stroma cells for scRNA-seq, mice were sacrificed via CO_2 asphyxia. Bones (femur and tibia) were harvested and placed in Media 199 (ThermoFisher Scientific, Ref#12350039) supplemented with 2% Fetal Bovine Serum (FBS, ThermoFisher Scientific, Ref#10082147). Muscle and tendon tissue was removed and bone marrow was flushed. Stromal cells from the bone marrow fraction were isolated by digestion with 1 mg/mL STEMxyme1 (Worthington, Ref#LS004106) and 1 mg/mL Dispase II (ThermoFisher Scientific, Ref#17105041), in Media 199 supplemented with 2% FBS for 25 min at 37°C. Stromal cells from the bone fraction were isolated by gently crushing and cutting bones (including epiphysis) into small fragments and digested in the same digestion mix as the bone marrow for 25 min, at 37°C with agitation (120 rpm). After digestions, both fractions were filtered through a 70 μm filter into a collection tube (Fisher Scientific, Ref#08-771-2), pooled into one sample or run separately (e.g., for bone versus bone marrow fraction scRNA-seq analysis), and erythrocytes lysed in ACK-lysis buffer (ThermoFisher Scientific, Ref#A1049201) for 5 minutes on ice. Cells were then stained in Media 199 supplemented with 2% FBS for FACS cell sorting.

FACS enrichment of bone marrow stromal cells

For flow cytometry and FACS, cells were resuspended in Media 199 supplemented with 2% FBS and stained for Ter119-APC (eBioscience, Ref#17-5921-82, clone TER-119), CD71-PECy7 (Biolegend, Ref#113812, clone RI7217), CD45-PE (eBioscience, Ref#12-0451-82, clone 30-F11), CD3-PE (Biolegend, Ref#100206, clone 17A2), B220-PE (Biolegend, Ref#103208, clone RA3-6B2), CD19-PE (Biolegend, Ref#115508, clone 6D5), Gr-1-PE (Biolegend, Ref#108408, clone RB6-8C5), and Cd11b-PE (Biolegend, Ref#101208, clone M1/70) for 30 minutes on ice. Dead cells and debris were excluded by FSC, SSC, 7-AAD (ThermoFisher Scientific, Ref#00-6993-50) and Calcein AM (ThermoFisher Scientific, Ref#C3099) profiles. FACS and cytometry was performed on a BD FACSAria II sorter, and sorted bone marrow stromal cells were collected in Media 199 supplemented with 2% FBS and 0.4% UltraPure BSA (ThermoFisher Scientific, Ref#AM2616). Bone marrow stroma was enriched by sorting of live cells (7-AAD-/Calcein+) negative for erythroid (CD71/Ter119) and immune lineage markers (CD45/CD3/B220/CD19/Gr-1/CD11b). For flow cytometric analysis (e.g., Figure S1K), we used Ly6a/Sca-1 (Biolegend, Ref#108127, clone), CD31 (Pecam1) (BD Bioscience, Ref#565097), Vcam1 (Biolegend, Ref#105710), CD34 (eBioscience, Ref#11-0341-82), Cdh5/CD144 (Biolegend, Ref#138006)

Immunostaining of bone marrow sections

Tissue preparation, immunostaining and imaging of full-bone femoral sections was performed as previously described (Coutu et al., 2018). Briefly, bones were fixed overnight in 4% paraformaldehyde and decalcified using 10% ethylenediaminetetraacetic acid (EDTA, pH = 8) for two weeks. Longitudinal bone sections were stained overnight at RT with primary [anti-CD31 (goat, R&D, Ref#AF3628), anti-IL6st (rat, eBiosciences, Ref#17-1302-82), anti-collagen type I (rabbit, Cedarlene, Ref#CL50151AP), anti-von Willenbrand factor (rabbit, Thermo Scientific, Ref#RB-281-AO), anti-Endomucin (rat, eBiosciences, Ref#14-5851-82)] and secondary antibodies (CF488, CF555, CF633 and CF680, Biotium). Detection of IL6st was performed by biotin-streptavidin CF555 amplification. Sections were then optically cleared using graded series of 2,2-thiodiethanol (TDE, Sigma).

Full-bone imaging was performed on a Leica TCS SP8 confocal microscope equipped with two photomultiplier tubes, three HyD detectors and three laser lines (405-nm blue diode, argon and white light) using type F immersion liquid (RI: 1.518) and 20X multiple immersion objective (NA 0.75, FWD 0.680 mm). Images were acquired at 8-bit, 400 Hz and 1024x1024 or 2048x2048 resolution with 2.49 μm z-spacing.

Single cell RNA-seq

Single cells were encapsulated into emulsion droplets using Chromium Controller (10x Genomics). scRNA-seq libraries were constructed using Chromium Single Cell 3′ v2 Reagent Kit according to the manufacturer's protocol. Briefly, post sorting sample volume was decreased and cells were examined under a microscope and counted with a hemocytometer. Cells were then loaded in each channel with a target output of ~4,000 cells. Reverse transcription and library preparation were performed on C1000 Touch Thermal cycler with 96-Deep Well Reaction Module (Bio-Rad). Amplified cDNA and final libraries were evaluated on a Agilent BioAnalyzer using a High Sensitivity DNA Kit (Agilent Technologies). Individual libraries were diluted to 4nM and pooled for sequencing. Pools were sequenced with 75 cycle run kits (26bp Read1, 8bp Index1 and 55bp Read2) on the NextSeq 500 Sequencing System (Illumina) to ~70%–80% saturation level.

QUANTIFICATION AND STATISTICAL ANALYSIS

Pre-processing of scRNA-seq data

ScRNA-Seq data were demultiplexed, aligned to the mouse genome, version mm10, and UMI-collapsed with the Cellranger toolkit (version 2.0.1, 10X Genomics). We excluded cells with fewer than 500 detected genes (where each gene had to have at least one UMI aligned). Gene expression was represented as the fraction of its UMI count with respect to total UMI in the cell and then multiplied by 10,000. We denoted it by TP10K – transcripts per 10K transcripts.

Dimensionality reduction

We performed dimensionality reduction using gene expression data for a subset of variable genes. The variable genes were selected based on dispersion of binned variance to mean expression ratios using *FindVariableGenes* function of *Seurat* package (Satija et al., 2015) followed by filtering of cell-cycle, ribosomal protein, and mitochondrial genes. Next, we performed principal component analysis (PCA) and reduced the data to the top 50 PCA components (number of components was chosen based on standard deviations of the principal components – in a plateau region of an "elbow plot").

Clustering and sub-clustering

We used graph-based clustering of the PCA reduced data with the Louvain Method (Blondel et al., 2008) after computing a shared nearest neighbor graph (Satija et al., 2015). We visualized the clusters on a 2D map produced with t-distributed stochastic neighbor embedding (t-SNE) (van der Maaten and Hinton, 2008). For sub-clustering, we applied the same procedure of finding variable genes, dimensionality reduction, and clustering to the restricted set of data (usually restricted to one initial cluster).

Differential expression of gene signatures

For each cluster, we used the Wilcoxon Rank-Sum Test to find genes that had significantly different RNA-seq TP10K expression when compared to the remaining clusters (paired tests when indicated) (after multiple hypothesis testing correction). As a support measure for ranking differentially expressed genes we also used the area under receiver operating characteristic (ROC) curve.

Filtering hematopoietic clusters and doublets

Based on cluster annotations with characteristic genes, we removed hematopoietic clusters from further analysis. It is further expected that a small fraction of data should consist of cell doublets (and to an even lesser extent of higher order multiplets) due to co-encapsulation into droplets and/or as occasional pairs of cells that were not dissociated in sample preparation. Therefore, when we found small clusters of cells expressing both hematopoietic and stromal markers we removed them from further analysis (original cluster 14). A small number of additional clusters and subclusters was marked by genes differentially expressed in at least two larger stromal clusters and were annotated as doublets if their average number of expressed genes was higher than the averages for corresponding suspected singlet cluster sources and/or they were not characterized by specific differentially expressed genes (original clusters 18 and 19). All marked doublets were removed from the discussion.

Impact of dissociation on clustering

We checked the possible impact of dissociation by several analyses. First, we re-ran the clustering of our dataset but after removing the known dissociation artifact genes (van den Brink et al., 2017) from the data matrix. We did not observe substantial clustering changes in this approach. Specifically, the number of clusters remained the same and 98% of cell pairs had the same cluster assignment. Second, we performed binning of cells into ''clusters'' based on the expression of *only* dissociation signature scores (with the same bin sizes as the real clusters): the adjusted random index between our full clustering and this binning was 0.009 (for equivalent clustering the value is 1). This indicated that our global clustering was not driven by the dissociation signature expression. Third, we repeated this test for clusters that were further subclustered. The values were: 0.242 (Lepr-MSC, cluster 1), 0.006 (OLC-1, cluster 7), 0.027 (OLC-2, cluster 8), and 0.024 (Perictyes, cluter 12). This indicated that only the subclustering of Lepr-MSC cells was possibly partially correlated with dissociation signature or other biological processes with correlated signatures (we note that immediate early gene expression is the main feature of the ''dissociation signature'' and can also be a biological phenomenon). For visual clarity we show in Figure S1J the expression of the dissociation signature score (Tirosh et al., 2016) across a tSNE plot of our cells.

Estimation of proliferation status

To score cells for their relative proliferation status, we used a set of characteristic genes involved in cell-cycle (Kowalczyk et al., 2015). For each cell we computed the average expression (TP10K) of cell-cycle genes as a proxy for proliferation status.

Diffusion maps computation and visualization

We performed non-linear dimensionality reduction of scRNA-seq data by restricting a sparse diffusion matrix of expression data to the eigenspace spanned by eigenvectors corresponding to the top diffusion matrix eigenvalues. We used the *destiny* package (Angerer et al., 2016), where we used the local estimation of Gaussian kernel width, and the number of nearest neighbors for diffusion matrix approximation was set to the smaller value between the square root of the number of all single cells in the data and 100. The diffusion matrix was constructed on sets of variable genes computed with the same procedure as the one used for clustering and sub-clustering of the data, such that variable genes were re-computed for each diffusion map.

We visualized diffusion maps following the approach described in Schiebinger et al. (2017). Specifically, we built a nearest-neighbor graph in the projected space using an implementation of k-NN algorithm from the package *FNN* (Beygelzimer et al., 2015), and then computed a force-directed layout using *ForceAtlas2* (Jacomy et al., 2014) from the *Gephi* package (Bastian et al., 2009).

Connectivity of cell clusters

We quantified the connectivity of single-cell clusters using the partition based graph abstraction method PAGA (Wolf et al., 2017), a part of the single-cell analysis package *Scanpy* (Wolf et al., 2018). The computations were carried out on the same subset of variable genes as for clustering, using default parameters.

Cell identity assignment in the leukemia data

For scRNA-seq data from control and leukemic mice, we removed hematopoietic cells from the data as described above, and assigned cell types/identities to each cell using differential expression signatures derived from steady state data. Specifically, we collected up to 50 top, most differentially expressed genes (Table S1) in each of the 20 original clusters from the homeostasis dataset as signatures. For each candidate cell, we computed its signature scores for ach of the 20 signatures. Each signature score was computed against a background gene set of randomly selected genes. A cell was assigned to the cell-type/cluster with the best signature score. When assigning the sub-cluster identity, we further scored against signature genes of sub-clusters (Table S2) that consisted of up to 20 most differentially expressed sub-cluster genes.

Changes in cluster sizes in leukemia data

For each cluster, we used the Wald test to quantify the association of condition (control, leukemia) with binomial models. Specifically, for each sample, we collected numbers of cells belonging to a given cluster and the number of cells outside of the cluster. Then we fit a generalized linear model with binomial parameters to the combined data with and without a parameter indicating condition (control, leukemia). We used an R implementation of Wald test to assess the statistical significance of the difference between the two models. Finally, we corrected the Wald test p-values from all clusters for multiple-hypothesis testing (Benjamini and Hochberg, 1995).

Differential expression in leukemia data

We observed some contamination of single cell data likely due to ambient RNA. Therefore, prior to computing differentially expressed genes between leukemia and control, we filtered out those genes that were differentially expressed in the hematopoietic contingent of the data when compared with the stromal contingent. The filtered genes were identified separately in leukemia and control conditions, since their respective hematopoietic contingents are known to be different. Specifically, this was achieved by computing differentially expressed genes using Bonferroni corrected Wilcoxon Sum-Rank Test as implemented in *FindAllMarkers* function (default parameters) of the Seurat package and excluding genes from hematopoietic clusters with adjusted p values < 0.05.

Then, separately for each cluster, we computed genes that were differentially expressed between leukemia and control in two ways. First, we used Bonferroni corrected Wilcoxon Rank-Sum Test (using *FindMarkers* of Seurat package, logfc.threshold = ln(1.2)) to discover differentially expressed genes between conditions. Second, for each cluster, we computed average TP10K expression of cells in every replicate. Then, we used those values in a t-test to assess differences between leukemia and control conditions. This approach mimicked bulk RNA-seq measurements. The second approach, although less powerful for discovery of differentially regulated genes, helped us to identify genes that tended to be coherently regulated in samples.

Gene set enrichment analysis

We used Gene Set Enrichment Analysis (GSEA) with MSigDB (Subramanian et al., 2005) gene sets to identify pathways and cellular states having induced or repressed expression in each cell cluster. Specifically, we used the pre-ranked analysis mode, with gene transcripts ranked according to differential expression analysis results (Wilcoxon Runk-Sum Test) of comparing leukemic and control conditions in each cluster. The most significantly overexpressed genes were placed at the top of the ranked list, while the most under-expressed were at the bottom before running the test.

Classify cells as having bone marrow origin

We used additional separate sequencing data samples from bone and bone marrow, together with a supervised classification strategy to determine tissue origin of cells in our original dataset. Specifically, we trained a multi-class Random Forest (RF) classifier using the R package "randomForest" (Liaw and Wiener, 2002) on a dataset of cells from bone and bone marrow, clustered separately. The RF classifier was trained on the subset of variable genes (determined with Seurat package) from all datasets, using 5000 trees. The number of training cells per cell cluster was sampled to a min of 70% of cluster size or 1000. The remaining cells comprised the test set and were predicted with an accuracy of 93.1%. The RF model was then used to predict the cluster of origin of every cell in our original dataset. Lineage identity was assigned based on lineage origin of predicted cell class.

DATA AND SOFTWARE AVAILABILITY

The scRNA-seq data generated in this study are deposited in GEO (GSE128423, https://www.ncbi.nlm.nih.gov/geo/query/acc.cgi?acc=GSE128423). Portals for browsing and exploring the entire atlas are available for steady-state (https://portals.broadinstitute.org/single_cell/study/mouse-bone-marrow-stroma-in-homeostasis) and leukemia (https://portals.broadinstitute.org/single_cell/study/mouse-bone-marrow-stroma-in-emergent-leukemia).

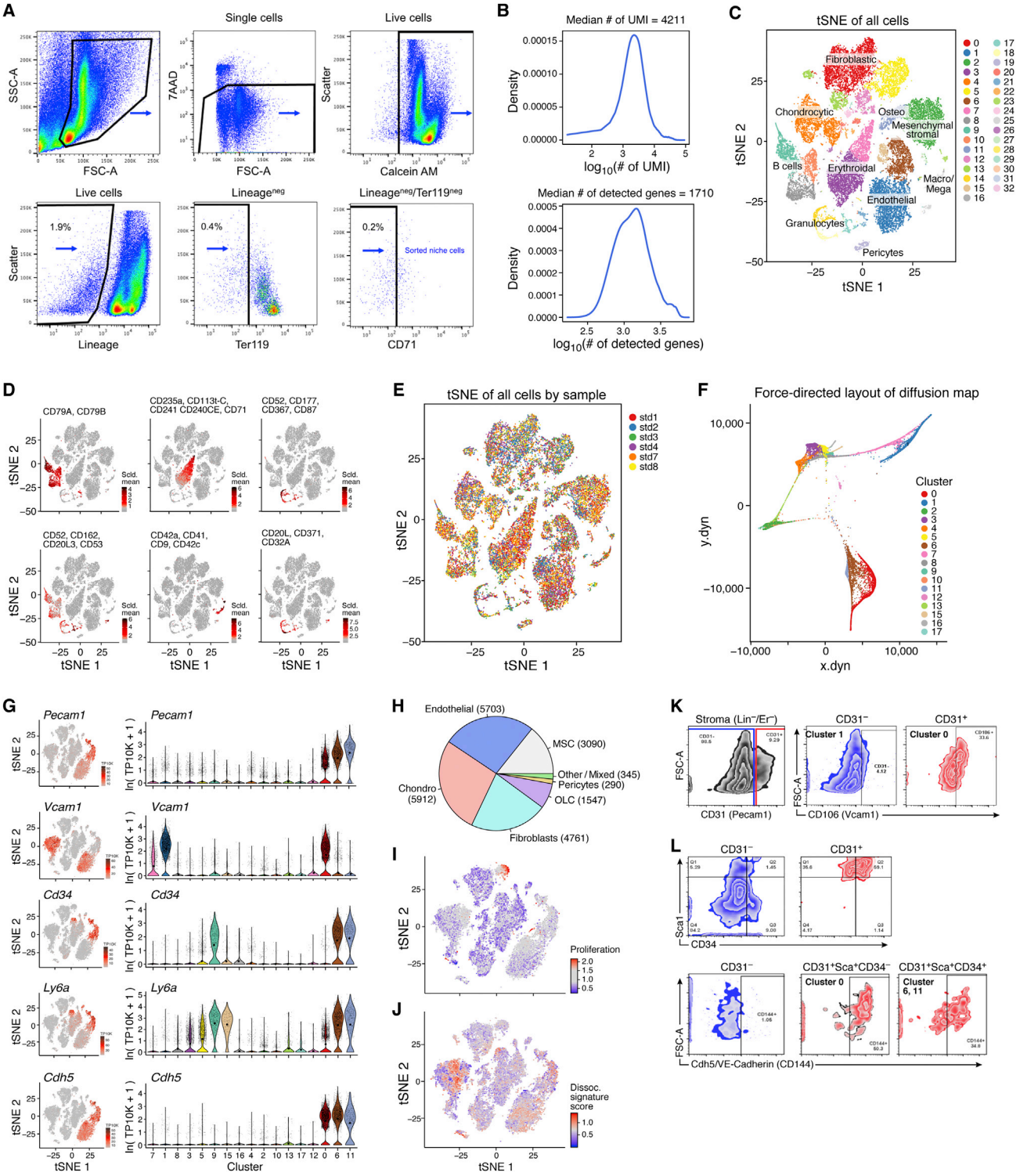

Figure S1. A Single-Cell Atlas of the Mouse Stroma, Related to Figure 1

(A) Gating strategy for isolation of mouse bone and bone marrow stroma. (B) RNA-seq data quality measures (UMI and genes in cells). (C) t-SNE map of the 30,543 bone and bone marrow cells (non- and hematopoietic) colored by clusters and annotated post hoc. Cells were partitioned into 33 clusters by unsupervised clustering (STAR Methods), annotated post hoc (STAR Methods) resulting in 20,896 cells in non-hematopoietic and 9,647 cells in hematopoietic clusters. (D) t-SNE maps as in C) but colored by average expression (color bar, TP10K) of hematopoietic signature genes. (E) As in C) but with colors marking samples. (F) A force directed layout embedding (FLE) of the cells (dots) from a diffusion map (50 components) computed with the cells from all stroma clusters. (G) Signature

(legend continued on next page)

genes for MSC and ECs. tSNE of Figure 1B colored by expression (color bar, TP10K) of key signature genes (left) (right), along with the corresponding distributions of expression levels (ln(TP10K+1), y axis) across the 17 clusters of Figure 1B (x axis). (H) Numbers of bone and bone marrow stromal cells in major cell types. (I) tSNE of Figure 1B colored by proliferation score (color bar, STAR Methods). (J) tSNE of Figure 1B colored by dissociation signature score (color bar, STAR Methods). (K,L) FACS analysis of Lepr-MSCs (cluster 1) and BMECs (cluster 0, 6, 11). Same strategy to enrich stroma from immune (Lin-) and erythroid (Er-) cells in (A) was used in combination with antibodies that label BMECs (CD31/*Pecam1*, Sca-1/*Ly6a*, CD34, VE-Cadherin/*Cdh5*), or MSCs (CD106/*Vcam1*). Cluster 1 cells were separated from all stroma clusters through combination of Lin-/Er-/CD31-/Vcam1+, and cluster 0 through Lin-/Er-/CD31+/Vcam1+. Cluster 6 and 11 were separated from cluster 0 through Lin-/Er-/CD31+/Sca1+/CD34+/VE-Cadherin+.

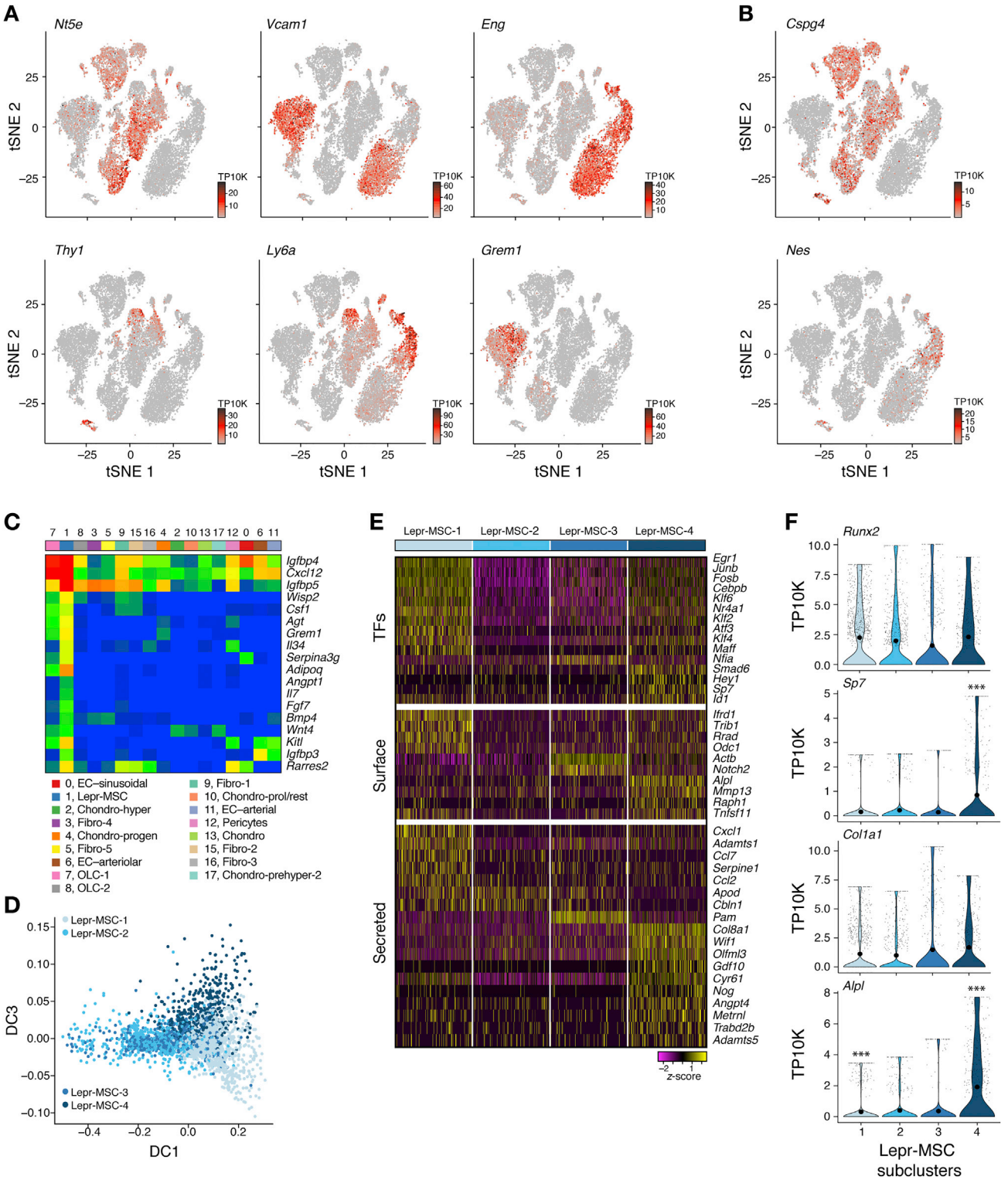

Figure S2. Four Subsets of HSC Regulator-Producing Lepr-MSCs Form a Differentiation Continuum, Related to Figure 2

(A,B) tSNE of Figure 1B colored by expression (color bar, TP10K) of select genes used in the field for labeling MSC populations. (C) Average expression (ln(TP10K+1)) in all bone and bone marrow stroma clusters of top secreted genes that were also differentially expressed in Lepr-MSCs (cluster 1). (D) Lepr-MSC sub-clusters diffusion map (2D projection, eigenvectors 1 and 3). (E). Expression (row-wide z-score of ln of TP10K, single cell view) of top differentially expressed genes (rows) across the cells (columns) in four major Lepr-MSC subclusters. (color bar, top, as in Figure 2E), ordered by three gene categories (labels on left). (F) Distributions of expression levels (TP4K, y axis, censored scale) for select marker genes across the four Lepr-MSC sub-clusters.

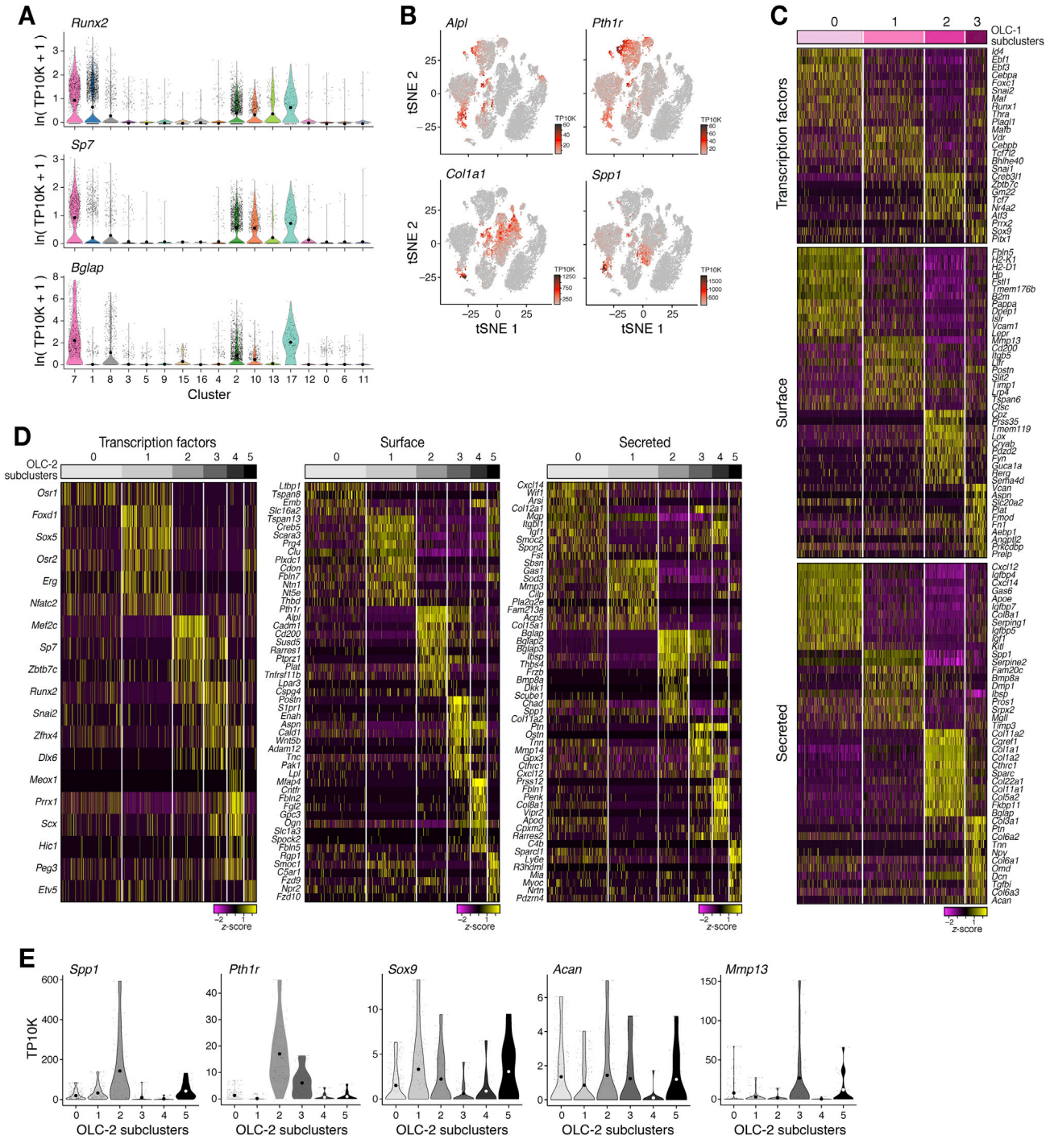

Figure S3. Two OLC Subsets of Distinct Differentiation Origins and Hematopoietic Support Potential, Related to Figure 3

(A) The distributions of expression levels (ln(TP10K+1), y axis) for genes as in Figure 3B across the 17 clusters of Figure 1B (x axis). (B) tSNE of Figure 1B colored by expression (color bar, TP10K) of select OLC related genes. (C) Expression (row-wide z-score of ln of TP10K, single cell view) of top differentially expressed genes (rows) across the cells (columns) in four OLC-1 subclusters. (color bar, top, as in Figure 3E), ordered by three gene categories (labels on left). (D) Expression (row-wide z-score of ln of TP10K, single cell view) of top differentially expressed genes (rows) across the cells (columns) in six OLC-2 subclusters. (color bar, top, as in Figure 3K), ordered by three gene categories (labels on top). (E) Distributions of expression levels (TP10K, y axis, censored scale) for select marker genes across the six OLC-2 sub-clusters.

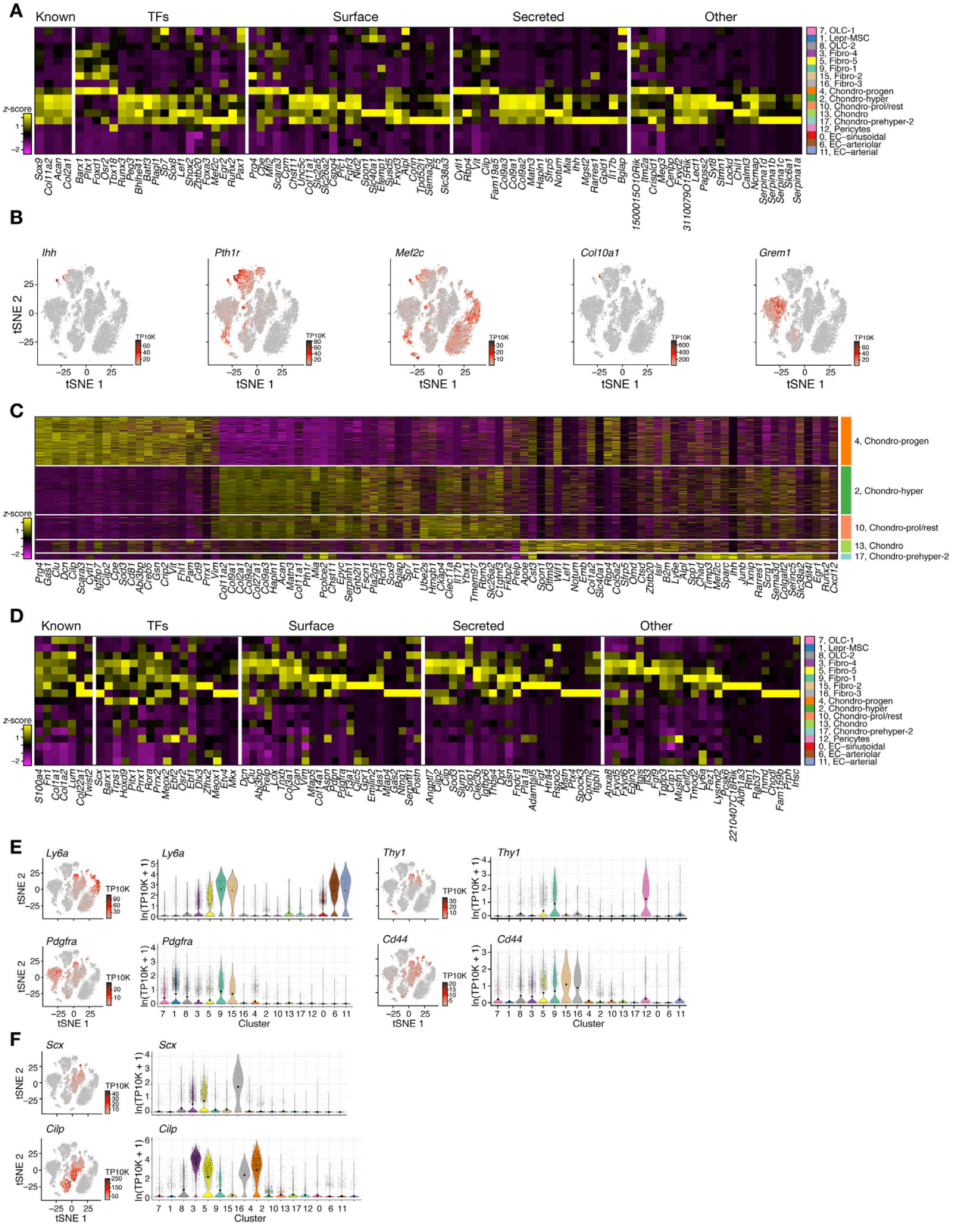

(legend on next page)

Figure S4. Chondrocyte and Fibroblasts Subsets Highlight Differentiation Paths and Hematopoiesis Support, Respectively, Related to Figure 4

(A) Expression (column-wide z-score of ln of average TP10K) of top differentially expressed chondrocyte genes (columns) ordered by five gene categories (labels on top) in the cells of each cluster (rows, color bar, right, as in Figure 1B). (B) tSNE of Figure 1B colored by expression (color bar, TP10K) of select genes used for chondrocyte identification. (C) Expression (column-wide z-score of ln of TP10K, single cell view) of top differentially expressed genes (columns) across the cells (rows) in chondrocyte clusters. (color bar, right, as in Figure 1D but only for chondrocyte clusters). (D) Expression (column-wide z-score of ln of average TP10K) of top differentially expressed fibroblast genes (columns) ordered by five gene categories (labels on top) in the cells of each cluster (rows, color bar, right, as in Figure 1B). (E,F) tSNE of Figure 1B colored by expression (color bar, TP10K) of select genes (left) (right), along with the corresponding distributions of expression levels (ln(TP10K+1), y axis) for the same genes across the seventeen clusters of Figure 1B (x axis).

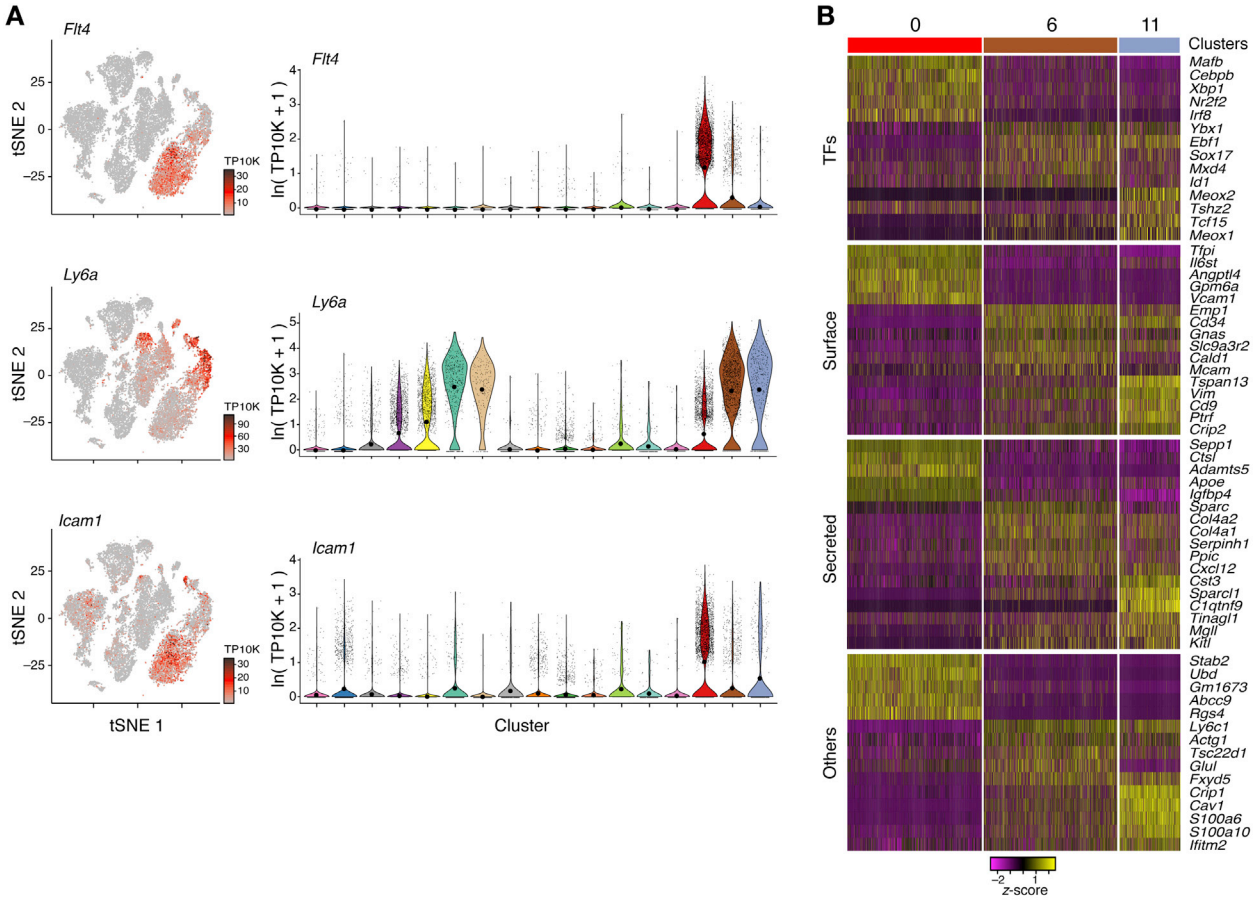

(legend on next page)

Figure S5. Arterial BMECs Express Higher Levels of Niche Factors Compared to Sinusoidal and Arteriolar Vascular BMECs, Related to Figure 5

(A) Signature genes for BMECs. tSNE of Figure 1B colored by expression (color bar, TP10K) of key BMEC marker genes (left) (right), along with the distributions of expression levels (ln(TP10K+1), y axis) for the same genes across the 17 clusters of Figure 1B (x axis). (B) Expression (row-wide z-score of ln of TP10K, single cell view) of top differentially expressed genes (rows) across the cells (columns) in BMEC clusters. (color bar, top, as in Figure 1D but only for EC clusters), ordered by four gene categories (labels on left). (C) Co-localization analysis in diaphysis showing that only 1.39% of the VWF+ vasculature voxels are also endomucin+. (D) *Tek* gene - the distributions of expression levels (ln(TP10K+1), y axis) across the 17 clusters of Figure 1B (x axis). (E) Volcano plot depicting changes in gene transcription (log2(fc), x axis; log10(adjusted p value), y axis) between arterial (cluster 11) and arteriolar (cluster 6) cells. Marked gene names had at least 2-fold expression change and adjusted p value < 0.001 and were expressed in at least 50% cells in one of the clusters. Insignificant genes with small fold changes (center of the volcano plot) were not included in the plot. Positive fold change indicates genes with higher average expression in arterioles (cluster 6).

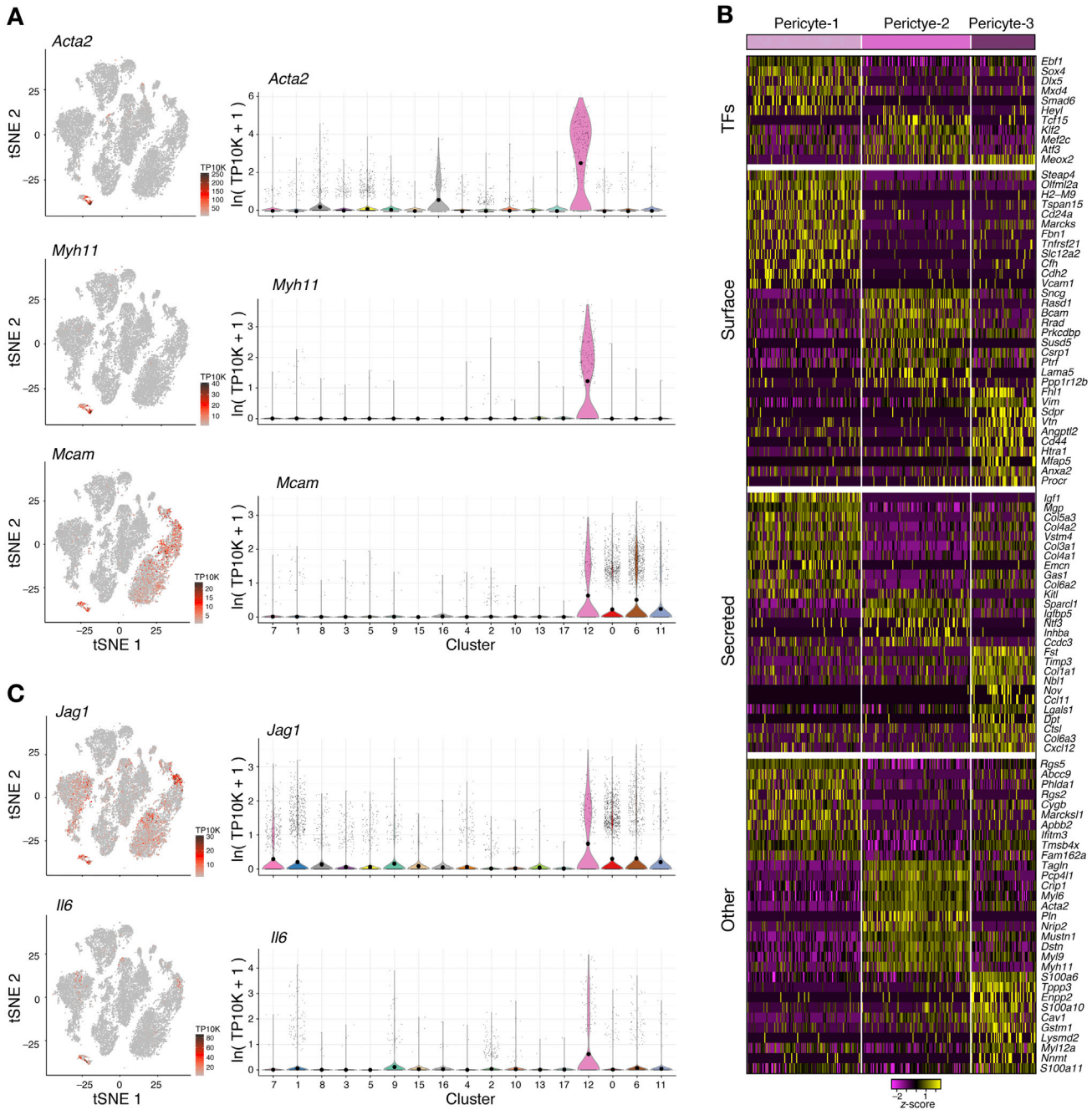

Figure S6. Three Distinct Subpopulations of Pericytes that Vary in Hematopoietic Regulatory Gene Expression, Related to Figure 6

(A,C) Signature genes for pericytes. tSNE of Figure 1B colored by expression (color bar, TP10K) of key marker genes (left) (right), along with the corresponding distributions of expression levels (ln(TP10K+1), y axis) across the 17 clusters of Figure 1B (x axis). (B) Top differentially expressed genes among pericyte subclusters (single cell view, relative expression z-score). Expression (row-wide z-score of ln of TP10K, single cell view) of top differentially expressed genes (rows) across the cells (columns) in pericyte subclusters. (color bar, top, as in Figure 6D), ordered by four gene categories (labels on left).

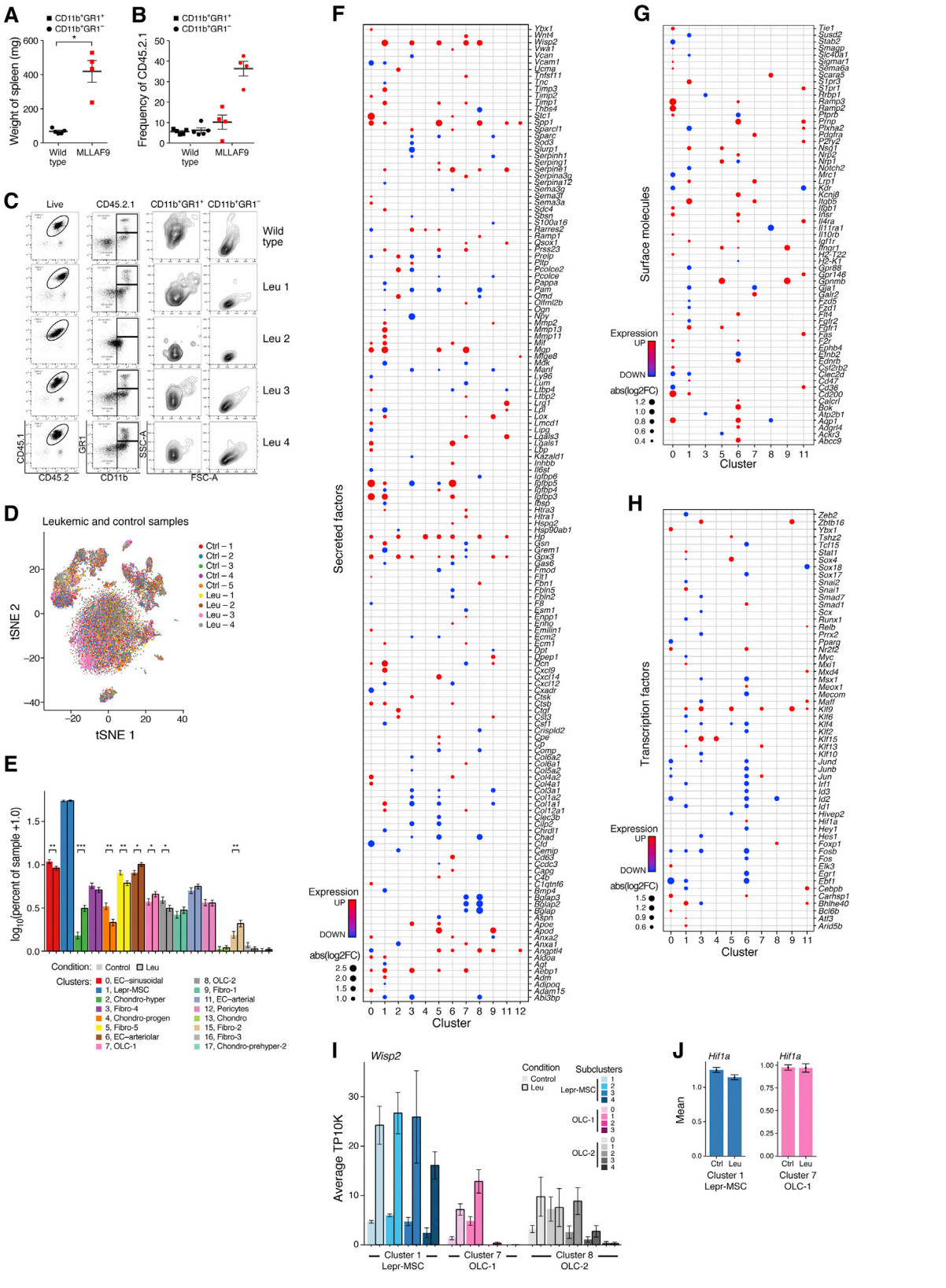

(legend on next page)

Figure S7. Remodeling of the Bone Marrow Stroma in Leukemia, Related to Figure 7

(A) Spleen weight of leukemic mice used for scRNA-seq experiments. Spleen weights for matched controls (n = 5) and leukemic mice (n = 4). (Student's t test, *$p < 0.05$). (B) Donor chimerism and leukemic blast appearance. (C) Frequency of myeloid cells in peripheral blood from wild-type control (top row) and MLL-AF9 leukemic mice (row 2-5) characterized by FACS analysis. (D) A census of the leukemic bone marrow stroma. tSNE of 23,004 cells (dots) from control and leukemic bone marrow colored by sample. (E) Compositional changes in bone marrow stroma. Binomial fit mean as percent of cells (y axis) assigned to specific cluster among control or leukemic samples (x axis). Error bars: 95% confidence interval of the binomial fit mean. (F-H) Fold changes of differentially expressed genes in leukemia. Adjusted p value < 0.05), up- (red) and down- (blue) regulated in leukemia. Dot size proportional to base-2 log of fold-change. G) As in F but for cell surface expressed genes. H) As in F but for transcription factor coding genes. (I) Changes in *Wisp2* expression in MSCs and OLCs. Average of samples (TP10K, y axis) in Lepr-MSC and OLC sub-clusters (x axis). Error bars: SEM (J) Changes in *Hif1a* expression in MSCs and OLC-1 s in leukemia. Average expression (TP10K, y axis). Error bars: SEM.